POLYMER HYDROGEL NANOPARTICLES AND THEIR NETWORKS

Xihua Lu, B.E., M.S.

Dissertation Prepared for the Degree of

DOCTOR OF PHILOSOPHY

UNIVERSITY OF NORTH TEXAS

August 2002

APPROVED:

Zhibing Hu, Major Professor
Nandika A. D'Souza, Committee Member
Samuel Matteson, Committee Member
Robert M. Wallace, Committee Member
Brace Gnade, Committee Member and Chairman
Department of Materials Science
C. Neal Tate, Dean of the Robert B. Toulouse
School of Graduate Studies

Lu, Xihua, Polymer hydrogel nanoparticles and their networks. Doctor of Philosophy (Materials Science), August 2002, 105 pp., 1 table, 29 illustrations, 98 references.

The thermally responsive hydroxypropyl cellulose (HPC) hydrogel nanoparticles have been synthesized and characterized. The HPC particles were obtained by chemically crosslinking collapsed HPC polymer chains in water-surfactant (dodecyltrimethylammonium bromide) dispersion above the lower critical solution temperature (LCST) of the HPC. The size distributions of microgel particles, measured by dynamic light scattering, have been correlated with synthesis conditions including surfactant concentration, polymer concentration, and reaction temperature. The swelling and phase transition properties of resultant HPC microgels have been analyzed using both static and dynamic light scattering techniques.

By first making gel nanoparticles and then covalently bonding them together, we have engineered a new class of gels with two levels of structural hierarchy: the primary network is crosslinked polymer chains in each individual particle, while the secondary network is a system of crosslinked nanoparticles. The covalent bonding contributes to the structural stability of the nanostructured gels, while self-assembly provides them with crystal structures that diffract light, resulting in colors. By using N-isopropylacrylamide copolymer hydrogel nanoparticles, we have synthesized nanoparticle networks that display a striking iridescence like precious opal but are soft and flexible like gelatin. This is in contrast to previous colored hydrogels, which were created either by adding dyes or fluorescent, or by organic solvent or by embedding a colloidal crystal array of polymer

solid spheres . Creating such periodic 3D structures in materials allows us to obtain useful functionality not only from the constituent building blocks but also from the long-range ordering that characterizes these structures.

Hydroxypropyl cellulose (HPC) and poly (acrylic acid) (PAA) complexes were studied using turbidity measurement and laser light scattering. The phase transition temperature of the complexes is found to depend on pH and molecular weights of PAA and HPC. The driving force for this phenomenon is due to the hydrogen bonding and hydrophobic interaction of the macromolecules. Based on the principle of the PAA/HPC complexes, the PAA nanoparticles were synthesized in 0.1wt % HPC aqueous solution at room temperature.

ACKNOWLEDGMENT

I am greatly indebted to my advisor Professor Zhibing Hu for his instruction and enthusiastic encouragement throughout this research. I particularly give my thanks to him for his financial support.

Special thanks are given to all the committee members for their advice.

The help of the warm support of other students in Dr. Hu's group is greatly acknowledged.

I should like to acknowledge my gratitude to my wife Hong Su for inestimable help and to my son Bowen Lu for his love.

I am grateful to support of this research by the U. S. Army Research Office under Grant No. DAAD 19-01-1-0596, the National Science Foundation under Grant No. DMR-0102468 , and the Petroleum Research Fund, administered by the American Chemical Society.

TABLE OF CONTENTS

LIST OF TABLE

Table Page

LIST OF ILLUSTRATIONS

CHAPTER 1

INTRODUCTION

Hydrogel nanoparticles (also called microgels) are crosslinked colloidal particles that can swell by the absorption of many times their weight of solvent (water). They exhibit a behavior ranging from that of polymer solutions to that of hard spheres.[1] Treating a dispersion of identical colloidal particles as a one-component assembly of superatoms dispersed in a continuous background, hydrogel nanoparticle systems lead to the fundamental study of modeling the transition from liquid to crystal and from the supercooled liquid to the glassy state of atomic fluids.[2] From an application point of view, the hydrogel nanoparticles can respond to environmental change much faster than the bulk gel due to the much smaller size of the particles. Unusual properties of the nanoparticles lead to various applications, including automotive surface coatings, printing, and controlled drug delivery.[3]

Many methods have been developed for preparing hydrogel nanoparticles, including emulsion polymerization,[4] inverse microemulsion polymerization, anionic copolymerization, and crosslinking of neighboring polymer chains. Currently, thermally-responsive hydrogel nanoparticles, as represented by N-isopropylacrylamide (NIPA) have attracted a great deal of attention due to their scientific importance and technological applications. The NIPA microgel was first synthesized by Pelton and

Chibante in 1986.[4] In their study, the pre-gel solution of the NIPA monomer was heated above the lower critical solution temperature (LCST) of the NIPA polymer solution. The polymerization of the NIPA monomers and crosslinking polymer chains occurred simultaneously at the reaction temperature T > LCST. Narrowly distributed NIPA hydrogel particles were obtained with their swelling properties similar to those of the bulk NIPA gel.

Hydrogels with nanometer-scale structures have been previously studied.[5,6] The nanostrucutred hydrogels with crystal structures were usually made: Nanoparticles were dispersed in the monomers and self-assembled to form periodical crystal structure through electrostatic repulsion, and then monomers were photopolymerized to form hydrogels and immobilize the ordered crystal structures. The major problem in previous work is that the nanoparticles embedded in the hydrogels are hydrophobic polymers like polystyrene. The interparticle distance can only be controlled by swelling and shrinking the hydrogel matrix.

This dissertation firstly investigates the synthesis and properties of hydroxypropyl cellulose (HPC) hydrogel nanoparticles. The HPC hydrogel nanoparticles were made directly from natural HPC polymer chains. Natural polymers are macromolecular structures in their original, while synthetic polymers are made from small molecules called monomers. The synthesis of the HPC nanoparticles will provide an important guide to preparation and study of other hydrogel nanoparticles directly from polymer chains. In contrast to most synthetic hydrogel nanoparticles that are made from carcinogenic or teratogenic monomers, the HPC nanoparticles comprise natural cellulose

ether macromolecules approved by the United State Food and Drug Administration (FDA) and thus have significant practical advantages over the synthetic hydrogel nanoparticles. Secondly, this dissertation contributes to novel nanostructured hydrogels --- hydrogel nanoparticle networks. Hydrogel nanoparticle networks are formed by covalently crosslinking nanoparticles, including the HPC nanoparticle network, the HPC nanoparticle co- poly(vinyl alcohol) (PVA) nanoparticle network, NIPA-co-AA (acrylic acid) copolymer nanoparticle network, and NIPA-co-HEAc (2-hydroxyethyl acrylate) copolymer nanoparticle network. Finally, the dissertation investigates the phase transition behavior of the HPC in the presence of poly(acrylic acid) (PAA). The phase transition of the HPC shifted to lower temperature in the presence of PAA at low pH. Dilute HPC/PAA solution can self-assemble to form the HPC/PAA hydrogel nanoparticles. The complexation between HPC and PAA at low pH leads to a new method of developing PAA microgels directly in aqueous solution. The dissertation has been divided into seven chapters. Chapter 2-7 are briefly described as follows:

In Chapter 2, the principle and application of laser light scattering are briefly reviewed.[7] In macromolecule and colloid science, laser light scattering (LLS)[8] is normally referred to the light scattering of the nonabsorbing macromolecules or colloidal particles. The two measurements of the LLS are respectively referred to as static (elastic, i.e., no absorption) and dynamic (quasi-elastic) laser light scattering (LLS). The static LLS measures the time-average scattered intensity, from which three parameters of macromolecules or colloidal particles, namely the weight-average molecular weight (M_w), the z-average root-mean-square radius of gyration ($<R_g^2>^{1/2}$,

simply R_g) and the second-order virial coefficient (A_2), can be obtained. Here, the second-order virial coefficient A_2 describes the interaction between a polymer and a solvent in the polymer solution. The dynamic LLS measures the intensity fluctuation (this is also where the word 'dynamic' comes from) and can be used to investigate the properties of the motion of the particles. The most commonly used method in dynamic LLS is the digital technique of photon correction spectroscopy (or optical mixing), which measures the intensity fluctuation of the scattered light in the time domain.

In Chapter 3, we report on the synthesis and study of another important thermally responsive microgel-- hydroxypropyl cellulose (HPC). Bulk HPC hydrogel, including the homogeneous gel and the porous gel have been extensively studied before.[9] The HPC gel collapses and shrinks above the volume phase transition temperature(T_c), around 41°C, but swells and expands below T_c.

To our knowledge, however, the synthesis of the HPC microgels has not been reported. In contrast to previous work on the NIPA microgel that started from NIPA monomers, we demonstrated a process whereby HPC chains in a surfactant solution were heated above the LCST to give colloidal particles that were then crosslinked to form microgel particles. In this chapter, our results will be divided into two parts. The first is to discuss synthesis of HPC microgels that involved fundamental interaction between high molecular weight polymer chains and surfactant. The second is to discuss swelling properties and the volume phase transition of HPC microgel particles as a function of temperature, crosslinker concentration and quality of solvent. Light scattering techniques have been used for both monitoring microgel formation and

characterizing the microgel particles. Such techniques have been widely used to study various microgels.[10]

In Chapter 4, novel nanostructured hydrogels are investigated. Polymer gels are a unique class of macromolecular networks that contain a large fraction of solvent within their structure. They are particularly suitable for biomedical applications because of their ability to simulate biological tissues.[11] In response to environmental stimuli such as temperature and pH, gels can reversibly swell or shrink up to 1000 times in volume and have varied applications such as artificial muscles, controlled drug release, and sensors.[12-15] Gels are usually formed by the free radical polymerization of monomers in the presence of a difunctional crosslinking agent. They can be made either in bulk or in nano- or micro-particles. The bulk gels are easy to handle, but have very slow swelling rate, while the gel nanoparticles act quickly to an external stimulus, but are too small for some applications. By first making gel nanoparticles and then covalently bonding them together, we have engineered a new class of gels with two levels of structural hierarchy: the primary network is the crosslinked polymer chains in each individual particle, while the secondary network is a system of crosslinked nanoparticles. Such nanostructured gels have new and unique properties that conventional gels do not have, including a high surface area, a bright blue color at room temperature, and temperature-tunable heterogeneity on the nanometer scale. This work may lead to creating opportunities for technological applications, ranging from controlled drug delivery, sensors, bio-adhesives, to displays.

In Chapter 5, we show a new class of bulk hydrogels with mesoscopical crystal structures. Hydrogels usually consist of randomly crosslinked polymer chains and contain a large amount of water filling interstitial spaces of the network, resulting in amorphous structures. Without a coloring agent, the hydrogels are clear when they fully swell in water. The central idea is to covalently bond self-assembled hydrogel nanoparticles. The covalent bonding contributes to the structural stability, while self-assembly provides the crystal structure that diffracts light, resulting in different colors. As a result, these novel materials, which contain up to 97 wt % water, display a striking iridescence, like precious opal, but are soft and flexible like gelatin. This is in contrast to previous colored hydrogels, which were created either by adding dyes or fluorescent molecules, organic solvents, or by embedding a colloidal crystal array of polymer solid spheres. In this chapter, three simple applications based on crystal hydrogels are presented: a gel sensor with environmentally-tunable colors, a gel "opal" that displays a striking iridescence but is elastic and soft, and a gel display whose iridescent pattern can be made either visible or invisible by simply switching temperature. Creating such periodic 3D structures in materials allows us to obtain useful functionality not only from the constituent building blocks, but also from the long-range ordering that characterizes these structures.[16]

In Chapter 6, the phase transition behavior of hydroxypropyl cellulose (HPC) in the presence of poly(acrylic acid) (PAA) is studied. Interpolymer complexes are physically interacting polymer chains in solution and have been extensively investigated.[17,18] The complexation of different polymers in solution is a commonly used procedure for

tailoring polymer properties to specific needs, without chemical modification of macromolecules. Most studies have been performed on the polymer complex systems, mainly focusing on the factors that affect complexation, including stoichiometric ratio of two complementary polymers, pH, ionic strength, solvent, concentration, and structure of the component polymers.[19, 20] However, only a few studies have been reported so far on the effect of complexation on the low critical solution temperature (LCST) of a nonionic polymer, that is the minimum point at which phase separation will invariably occur in a polymer solution. Hence, for a model study, we have chosen hydroxypropyl cellulose (HPC) as a proton-accepting polymer and poly(acrylic acid) (PAA) as a proton-donating polymer to study how the complexation between these two polymers affect the LCST of the HPC polymer under various conditions.

HPC exhibits a lower critical solution temperature (LCST) at 41 ^{0}C, and remarkable hydration-dehydration changes in aqueous solution in response to relatively small changes in temperate around the LCST. [21] Below the LCST, the HPC chains hydrate to form an expanded structure; above the LCST, the HPC chains dehydrate to form a shrinken structure. This property is due to the reversible formation and cleavage of the hydrogen bonds between the HPC and surrounding water molecules with changing temperature. The swelling behavior of HPC bulk gels, microgels, as polymer chains have been previously reported.[22,23] It is well known that incorporating hydrophobic comonomers leads to a lower LCST, and incorporating hydrophilic comonomers leads to a higher LCST. The changes in LCST caused by incorporating comonomers are due to changes in the overall hydrophilic properties of the polymer. This effect has been

investigated for another important thermally responsive polymer N-isopropylacrylamide (NIPA).[24]

We will show that based on complexation between the HPC and the PAA, the LCST of the HPC can be drastically changed. Studies of the structure and properties of interpolymer complexes between poly(acrylic acid) and nonionic cellulose ethers have been reported.[25-28] Specifically, Budtova and coworkers[29] investigated the formation and properties of the interpolymer complexation between PAA and cellulose ethers including hydroxyethylcellulose (HEC) and methylcellulose (MC). Their experimental results showed that the mixtures of the cellulose ethers and non-ionized PAA in aqueous solution formed interpolymer complexes due to hydrogen bonding. However, to our knowledge, systematic studies of the phase transition behavior of the HPC/PAA complex with change of pH have not been reported. In this chapter, the results of phase transition behavior of HPC/PAA complex in water will be given, studied by turbidity and dynamic laser light scattering measurements as functions of polymer concentration, temperature, pH value, and macromolecular weight.

The complexation between the HPC and the PAA also leads to a new method for the formation of surfactant-free PAA nanoparticles directly in aqueous media at room temperature. Such nanoparticles have very narrow size distributions as characterized by light scattering techniques, and can reversibly swell and shrink in response to external stimuli such as pH. These nanoparticles may be used as building blocks for the formation of nanoparticle networks[30] or carriers for controlled drug delivery.

In Chapter 7, the main conclusions of this dissertation are summarized.

REFERENCES

(1) Pelton, R. *Adv. Colloid Interf. Sci.* **2000**, *85*, 1.

(2) Senff, H.; Richtering, W. *J. Chem. Phys.* **1999**, *111*, 1705.

(3) Kiser, P. F.; Wilson, G.; Needham, D.; *Nature* **1998,** *394*, 459.

(4) Pelton, R.H.; Chibanate, P. *Colloids Surf.* **1986**, *120*, 247.

(5) Weissman, J. M.; Sunkara, H. B.; Tse, A. S.; Asher, S. A. *Science* **1996**, *274*, 959.

(6) Liu, L.; Li, P.; Asher, S. A. *Nature* **1998**, *397*, 141.

(7) Chu, B. *Laser Light Scattering*, 2nd edition; Academic Press, **1991**.

(8) Tanaka, T. *Experimental Methods in Polymer Science*; Academic Press, **2000**.

(9) Kabra, B. G.; Gehrke, S. H.; Spontak, R. J. *Macromolecules* **1998**, *31*, 2166.

(10) Zhou, S; Chu, B. *J. Phys. Chem*. **1998**, *102*, 1364.

(11) Peppas, N. A.; Langer, R. *Science* **1994,** *263*, 1715.

(12) Tanaka, T. *Phys. Rev. Lett*. **1978**, *40*, 820.

(13) Chen, G.; Hoffman, A. S. *Nature* **1995,** *373,* 49.

(14) Osada, Y.; Gong, J. P. *Adv. Mater*. **1998**, *10,* 827.

(15) Hu, Z.; Zhang, X.; Li, Y. *Science* **1995,** *269*, 525.

(16) Xia, Y.; Gates, B.; Yin, Y.; Lu, Y. *Adv. Mater*. **2000**, *12*, 693; Xia, Y. *Adv. Mater*. **2001**, *13*, 369.

(17) Tshuchi, E; Abe, K. *Adv. Polym. Sci*. **1982**, *45*, 1.

(18) Jiang, M.; Li, M.; Xiang, M.; Zhou, H. *Adv. Polym. Sci.* **1998,** *146,* 121.

(19) Dan,Y.; Chen, S. Y.; Zhang, Y. F.; Xiang, F. R. *J. Polym. Sci. Part B-Polym. Phys*. **2000,** *38*, 1069.

(20) Kaczmarek, H.; Szalla, A.; Kaminska, A. *Polyme*r **2001**, *42*, 6057.

(21) Gao, J.; Haidar, G.; Lu, X. H.; Hu, Z. B. *Macromolecules* **2001**, *34*, 2242.

(22) Harsh, D.C.; Gehrke, S.H. *J. Controlled Release* **1991**, *17,* 175.

(23) Lu, X. H.; Hu, Z. B.; Gao, J. *Macromolecules* **2000**, *33*, 8698.

(24) Shibayama, M.; Ikkai, F.; Inamoto, S.; Nomura, S.; Han, C. C. J. *Chem. Phys.***1996**, *105*, 4358.

(25) Barkalow, D. G.; Richey, L. C.; Zuehlke, J. W. *US 6303159*.

(26) Nikolaeva, O.; Budtova, T.; Alexeev, V.; Frenkel, S. *J. Polym. Sci.: Part B: Polymer Physics* **2000**, *38*, 1323.

(27) Nikolaeva, O. V.; Budtova, T. V.; Kalyuzhnaya, L. M.; Bel'nikevich, N. G.; Vlasova, E. N.; Frenkel, S. Y. *Polymer Science*, *Ser. A* **1999**, *41*, 771.

(28) Doseva, V; Senkov, S.; Baranovsky, Y. V. *Polymer* **1997,** *38*, 1339.

(29) Staikos, G.; Bokias, G.; *Macromol. Chem.* **1991**, *192*, 2649.

(30) Hu, Z.; Lu, X.; Gao, J.; Wang, C. *Advanced Materials* **2000,** *12***,** 1173.

CHAPTER 2

PRINCIPLE AND APPLICATION OF LASER LIGHT SCATTERING

2.1 Introduction

Laser light scattering (LLS) can be classified as elastic (no absorption) and inelastic (absorption, e.g., fluorescence, phosphorescence, and Raman) light scattering. In macromolecule and colloid science, laser light scattering normally refers to light scattering of nonabsorbing macromolecules or colloidal particles. When a monochromatic, coherent beam of light passes through a dilute macromolecular solution, or a suspension of colloidal dispersion, and the refractive index of the solute (macromolecules or colloidal particles) is different from that of the solvent, the incident light can be scattered by each macromolecule or particle in all directions. This scattered light contains information on the macromolecules or particles in solution, such as the size, the molar mass, and the conformation of the macromolecules or particles. By placing a detector (e.g., a photon multiplier tube) at a distance and focusing it on a small volume of scattered medium, you can obtain information about the macromolecules or the colloidal particles in solution from two different measurements: measurement of the time-average scattered intensity $<I>$ of photon counts $<n>$ and the fluctuation of $I(t)$ or $n(t)$ with time. In polymer and colloid science, these two measurements are respectively referred to as static (elastic, i.e., no absorption) and dynamic (quasi-elastic) laser light scattering (LLS).

If all the macromolecules or particles are stationary, the scattered light intensity at each direction will be a constant, i.e., independent of time. In reality, all the scatterers in solution are undergoing constant Brownian motion. This Brownian motion leads to a fluctuation of the scattered intensity pattern. The fluctuation rate can be related to different kinds of relaxation processes such as diffusion (transition and rotation) and internal motions of the macromolecules. The faster the relaxation process, the faster the intensity fluctuation may be.

The static LLS measures the time-average scattered intensity, whereas the dynamic LLS measures the intensity fluctuation (this is also where the word 'dynamic' comes from). The dynamic LLS is essentially caused by the Doppler effect. When an incident light is scattered by a moving macromolecule or particle, the frequency of the scattered light will be slightly higher or lower than that of the incident light, depending on the distance between the detected particle and the detector. Thus, for a macromolecule solution or a colloid dispersion, the frequency distribution of the scattered light is slightly broader than that of the incident light. This is why the dynamic LLS is also called quasi-elastic light scattering (QELS). The frequency broadening ($\approx 10^5$-10^7 Hz) is so small in comparison with the incident light frequency ($\approx 10^{15}$ Hz), it is very difficult to detect it in the frequency domain. However, it can be effectively recorded in the time domain through a time correlation function. For this reason, dynamic light scattering is sometimes referred to as photon correlation spectroscopy (PCS).

The static LLS is used in measuring time-average scattered intensity at different angles and concentrations, from which three parameters of macromolecules, namely the

weight-average molecular weight (M_w), the z-average root-mean-square radius of gyration ($<R_g^2>^{1/2}$, simply R_g), and the second-order virial coefficient (A_2) can be obtained. The dynamic LLS is designed to measure the fluctuation of scattered intensity. Translational diffusion coefficient (D), relaxation rate (Γ), hydrodynamic radius can be obtained from dynamic LLS. In the last two decades, thanks to the advance of laser technology, ultra-fast electronics and personal computers, LLS, especially dynamic LLS, has evolved from a very special instrument for fundamental research work to a routine analytical tool in polymer laboratories. It is even used as a quality-control device in production lines. Commercially available LLS instruments are normally capable of making both static and dynamic measurements simultaneously to study colloidal particles or macromolecules in solutions, as well as in gels and viscous media.

2.2 Static Laser Light Scattering[1-2]

In a real static LLS measurement of macromolecules or particles, two kinds of interference must be considered. One is the inner interference arising from different parts of a larger (dimension > $\lambda/10$) particle, whereas the intraparticle interference from small particles (dimension < $\lambda/10$) may be neglected. The other is from the interparticle interference between different particles. For dilute solutions, the interparticle interference could be neglected.

The Rayleigh ratio is a very important factor in static LLS, defined as

$$R = \frac{Ir^2}{I_0} \qquad (2-1)$$

where I is the scattered intensity per unit scattering volume, I_0 is the incident light intensity, and r is the average distance between the scatterers and the observer. Thus, the dimension of the Rayleigh ratio R is the reciprocal of the dimension of length. Based on the electromagnetic principle and concentration fluctuation theory, we can get the excess Rayleigh ratio of the dilute solution (R_{excess}):[2]

$$R_{excess} = \frac{I_{excess} r^2}{I_0} = \frac{4\pi^2 n^2}{\lambda_0^4} \left(\frac{dn}{dC}\right)^2 \frac{kTC}{\partial \Pi / \partial C} \qquad (2-2)$$

Where I_{excess} ($=I_{\text{solution}}$-I_{solvent}) is the net scattering intensity of the solute by subtracting the intensity of solvent from that of the solution, and n, λ_0, C, k, T, Π are the refractive index of the solution, the wave length of the incident light, the concentration of the solute, the Boltzmann constant, the absolute temperature, and the osmotic pressure, respectively.

For dilute macromolecule or particle solutions, the change of osmotic pressure induced by the change in concentration can be written[3]

$$\frac{\Pi}{C} = \frac{N_0 kT}{M}(1 + A_2 CM + \cdots) \qquad (2-3)$$

Thus
$$\frac{\partial \Pi}{\partial C} = \frac{N_0 kT}{M}(1 + 2A_2 M + \cdots) \qquad (2-4)$$

where N_0, M, and A_2 are the Avogadro's number, the weight-average molecular weight, and the second –order virial coefficient, respectively.

By substitution of equation (2-4) into equation (2-2), we can get the excess Rayleigh ratio:

$$R_{excess} = \frac{4\pi^2 n^2}{\lambda_0^{\,4} N_0}\left(\frac{dn}{dC}\right)^2 \frac{CM}{1 + 2A_2 CM + \cdots} \qquad (2-5)$$

R_{excess} is the net scattering intensity of the solute by subtracting the intensity of solvent from that of the solution. By defining $K = 4\pi^2 n^2 (dn/dC)^2 / (N_0 \lambda_0^4)$, we get

$$\frac{KC}{R} = \frac{1}{M} + 2A_2 C + \cdots \qquad (2-6)$$

where we have omitted the footnote "excess" in $R_{\text{excess.}}$ For larger macromolecules or colloidal particles, a construction factor must be introduced. Here, P(θ) is defined as an angular scattering function

$$P(\theta) = \frac{R(\theta)}{R(0)} = 1 - \frac{1}{3} q^2 < R_g^{\,2} > \qquad (2-7)$$

where $q = 4\pi n \sin(\theta/2)/\lambda$ is the magnitude of the scattering vector, $<R_g^2>$ is the mean square of the radius of gyration. Thus,

$$\frac{KC}{R(\theta)} = \frac{1}{MP(\theta)} + 2A_2 C \qquad (2-8)$$

when the concentration $C \rightarrow 0$,

$$R(\theta) = KCMP(\theta) = KCM\,[1-(1/3)q^2 <R_g^2> + \cdots]$$

$$\frac{R(\theta)}{KC} = M_w [1 - \frac{1}{3} q^2 < R_g^{\,2} >_z + \cdots] \qquad (2-9)$$

When $q^2 <R_g^2> << 1$, omitting the higher order (>2) terms in series, we get

$$\frac{KC}{R(\theta)} = \frac{1}{M_w}[1 + \frac{1}{3} q^2 < R_g^{\,2} >_z] + 2A_2 C \qquad (2-10)$$

This is the basic equation of static LLS which is frequently shown in the literature.[4-6]

It should be noted that Equation (2-10) is valid under the restriction that the polymer solution exhibits no adsorption, no fluorescence, and no depolarized scattering. Naturally, the molar mass in the equation, $M_w = \sum_i C_i M_i / \sum_i C_i$, is the weight-average; and the mean square radius of gyration, $< R_g^{\ 2} >_z = \sum_i C_i M_i R_{g,i}^{\ 2} / \sum_i C_i M_i$, is the z-average. It can be seen that when $R(\theta)$ is measured at a series of C and q, we are able to determine $<R_g^2>_z$ from the slope of $[KC/R(\theta)]_{c\to 0}$ versus q^2; A_2 from the slope of $[KC/R(\theta)]_{\theta\to 0}$ versus C; and M_w from $[KC/R(\theta)]_{c\to 0,\ k\to 0}$. In practice, the Rayleigh ratio is determined by a relative method; namely, by measuring the scattering intensity of a standard solvent such as benzene or toluene, we can calculate the Rayleigh ratio of a given solution by

$$R_{vv}(\theta) = R^o_{vv}(\theta)\frac{I(\theta)_{solution} - I(\theta)_{solvent}}{I(\theta)_{standard}}\left(\frac{n_{solvent}}{n_{standard}}\right)^{\gamma} \qquad (2-11)$$

The subscript "vv" means both the incident and the scattered light are vertically polarized; I and n are, respectively, the time-averaged scattering intensity and the refractive index. The term $(n_{solvent}/n_{standard})^{\gamma}$ is a refraction correction for the scattering volume and γ is a constant between 1 and 2, depending on the detection geometry of the light scattering instrument, because we should compare the same scattering volumes from the solution and the reference standard.

2.3 Dynamic Laser Light Scattering

Dynamic LLS can be used to study the properties of the motion of the particles.[7,8] The motion of the particles includes transitional, rotational or internal motion. The moving macromolecules or particles scatter the incident light passing through the macromolecules or particles and result in two main effects: the fluctuation of the scattered intensity and the broadening of the frequency distribution. In frequency domain, the frequency shift of the scattered light is very difficult to precisely detect, because the frequency broadening ($\approx 10^5$-10^7 Hz) is much smaller than the incident light frequency ($\approx 10^{15}$ Hz). However, in the time domain, the fluctuation of the scattered intensity is closely related to the frequency broadening and can be detected if the detector is sensitive enough and has a fast responsive time. It is equally efficient to have either the fluctuation of the scattered intensity or the frequency broadening because the two effects are related to each other. For an extremely dilute macromolecular or colloidal particle system, we don't consider the fluctuation of scattered intensity caused by the change in the number of the macromolecules or colloidal particles. The most commonly used method in quasi-elastic light scattering (QELS) is the digital technique of photon correction spectroscopy (or optical mixing) which measures the intensity fluctuation of the scattered light in the time domain. There are two basic forms of the optical mixing: heterodyne and homodyne (self-beating). Heterodyne mixing is the mixture of the scattered light with a reference beam (local oscillator) unshifted in frequency from the incident light beam. In self-beating optical mixing the scattered

wave is not mixed with a reference signal but directly detected. We will describe only the self-beating intensity-intensity time correction spectroscopy. It is worth to mentioning that averaging the detected intensity in dynamic LLS with time is the same as static LLS.

The Siegert relation is an important equation in dynamic LLS. When the scattered field is a Gaussian process, the correlation functions $g^{(1)}(t)$ and $g^{(2)}(t)$ are connected through the Siegert relation[2]

$$g^{(2)}(t) = 1 + | g^{(1)}(t) |^2 \qquad (2\text{-}12)$$

where $g^{(1)}(t) \equiv [\langle E(0)E^*(t)\rangle / \langle E(0)E^*(0)\rangle]$ and $g^{(2)}(t) \equiv [\langle I(0)I(t)\rangle / \langle I(0)\rangle^2]$ are the normalized field-field and normalized intensity-intensity autocorrelation functions, respectively. Thus, the intensity-intensity time autocorrelation function becomes

$$G^{(2)}(t) = \langle I(0)I(t)\rangle = \langle I(0)\rangle^2 g^{(2)}(t) = \langle I(0)\rangle^2 [1 + | g^{(1)}(t) |^2] \qquad (2\text{-}13)$$

The significance of introducing $g^{(2)}(t)$ and $G^{(2)}(t)$ lies in that $G^{(2)}(t)$ and $\langle I(0)\rangle$ can be measured experimentally. In practice, the detection area can not be zero. Therefore, the scattered light can't be purely coherent and an instrument parameter, β (<1), is introduced in equation (2-14)

$$G^{(2)}(t) = A [1 + \beta | g^{(1)}(t) |^2] \qquad (2\text{-}14)$$

where $A(\equiv\langle I(0)\rangle^2)$, t, and β are the measured baseline, the delay time, and the parameter depending on the coherence of the detection optics, respectively, and $I(t)$ is the scattered intensity, or photon counts, at time t, which includes contributions from both the solvent and the solute. Therefore,

$$G^{(2)}(t) = \langle I(0)I(t)\rangle = \langle [I_{solvent}(0) + I_{solute}(0)][I_{solvent}(t) + I_{solute}(t)]\rangle$$

and equation (2-12) becomes

$$[G^{(2)}(t) = A\{1 + \beta[\frac{I_{solvent}}{I_{solution}} \mid g^{(1)}_{solvent}(t) \mid + \frac{I_{solute}}{I_{solution}} \mid g^{(1)}_{solute}(t) \mid]^2 \qquad (2-15)$$

where all the cross terms disappear since the light scattered by solvent molecules and solute particles are not correlated. It should be noted that $\mid g^{(1)}_{solvent}(t) \mid$ decays much faster than $\mid g^{(1)}_{solute}(t) \mid$ because small solvent molecules diffuse faster than particles do. Thus, after a very short delay time, equation (2-13) becomes[1]

$$G^{(2(}(t) = A[1 + \beta(\frac{I_{solute}}{I_{solution}})^2 \mid g^{(1)}_{solute}(t) \mid^2] = A[1 + \beta_{app} \mid g^{(1)}_{solute} \mid^2] \qquad (2-16)$$

where $\beta_{app} = \beta(I_{solute} / I_{solution})^2$. For a dilute solution, the scattered intensity from solvent molecules could become appreciable, i.e., $I_{solute} \leq I_{solution}$, so that the apparent coherence β_{app} would be even lower, i.e., $G^{(2)}(0)$ appears to have a lower value than expected. We should be aware of this situation, especially for the weakly scattered, dilute, and low molar mass polymer solutions. For example, if $I_{solute} = I_{solvent}$, $\beta_{app} = \beta/4$. It should be noted that β is constant for each particular optical geometry of the scattering instrument. In fact, I_{solute} can be estimated from β_{app} (certainly I_{solute} can be measured in static LLS by comparing the scattered intensity of solution and solvent.) if the values of β at different scattering angles have been pre-calibrated with a narrowly distributed latex standard whose scattering intensity is much stronger than water (solvent).

Now we will see how to get the information about the motion of the particles from the measured intensity-intensity time correlation function $G^{(2)}(t)$. Generally, the

relaxation of $|g^{(1)}(t)|$ includes both diffusion (translation and rotation) and internal motions. Let us only consider the translational diffusion relaxation of the particles. For monodisperse, spherical scatterers, $|g^{(1)}(t)|$ is theoretically represented as an exponential decay function:

$$|g^{(1)}(t)| = G\, e^{-\Gamma t} \qquad (2\text{-}17)$$

where G and Γ are the factor of proportionality and the line-width, respectively and $\Gamma^{-1} = \tau_c$, the characteristic decay time representing the rate of dynamic relaxation in self-beating. For a polydisperse polymer sample with a continuous distribution of molar mass M, equation (2-17) may be generalized as

$$| g^{(1)}(t) = \int_0^\infty G(\Gamma) e^{-\Gamma t} d\Gamma \qquad (2-18)$$

where $G(\Gamma)$ is called the line-width distribution and $G(\Gamma)d\Gamma$ is the statistic weight of the particles or macromolecules which possess line-width Γ. By using a Laplace inversion program, CONTIN,[10,11] the normalized distribution function of the characteristic line width $G(\Gamma)$ was obtained. For a dilute solution, Γ measured at a finite scattering angle is related to C and q by

$$\frac{\Gamma}{q^2} = D(1 + k_d C)(1 + fq^2 < R_g^{\,2} >_z) \qquad (2-19)$$

where D is the transitional diffusion coefficient of the solute molecule at $C \rightarrow 0$, k_d is the diffusion second virial coefficient, and f is a dimensionless parameter depending on polymer chain structure and solvent (For polymers with flexible chains in a good solvent, f is between 0.1 and 0.2). Hence, for small C and q, $D \approx \Gamma/q^2$. It should be noted that by the definition of $|g^{(1)}(t)|$, $G(D) = q^2 G(\Gamma)$, the translational diffusion

coefficient distribution, is an intensity distribution. And, since $|g^{(1)}(t)|$ approaches unity as $t \rightarrow 0$, we have

$$| g^{(1)}(t \rightarrow 0) = \frac{< E(0)E^*(t \rightarrow 0) >}{< E(0)E^*(0) >} = \int_0^\infty G(\Gamma)d\Gamma = \int_0^\infty G(D)dD = 1$$

Here, the average diffusion coefficient $<D>$ is defined as

$$< D >= \int_0^\infty G(D)DdD \qquad (2-20)$$

Further, the transitional diffusion coefficient D may be related to the molecular friction factor f through the Stokes-Einstein relation

$$D = k_B T / f \qquad (2\text{-}21)$$

where k_B and T are the Boltzmann constant and the absolute temperature, respectively. For a hard sphere with a radius of R, $f = 6\pi\eta R$, where η is the viscosity of the solvent. For a polymer coil, R is replaced by its hydrodynamic radius R_h, so that

$$R_h = \frac{k_B T}{6\pi\eta D} \qquad (2-22)$$

In dynamic light scattering, translational motion of macromolecules or particles within size range of 1-1,000 nm can be measured. The characteristic time (τ_c) of dynamic relaxation in self-beating, which includes transitional , rotational, and internal motion, could very from seconds to tens of nanoseconds.

Dynamic LLS plays a very important role in particle sizing. [4-6, 9] In a dilute dispersion, if the colloidal particles are spherical, or in other words, in the absence of rotational and internal motions, $G(\Gamma)$ can be converted to the hydrodynamic size distribution $f(R_h)$. All the parameters in the conversion are either well-known constants

or precisely measurable by the other methods. Therefore, particle sizing based on dynamic LLS can be considered as an absolute method without calibration. This is why dynamic LLS is so successful in particle sizing and many commercial instruments have been developed using the dynamic LLS principle.

2.4 LLS Instrumentation

A commercial laser light scattering (LLS) spectrometer (ALV/DLS/SLS-5000) equipped with an ALV-5000 digital time correlator was used with a Helium-Neon laser (Uniphase 1145P, output power of 22mW and wavelength of 632.8 nm) as the light source (Figure 2.1). The incident light was vertically polarized with respect to the scattering plane and the light intensity was regulated with a beam attenuator (Newport M-925B). The scattered light was transmitted through a very thin(~ 40 μm in diameter) optical fiber leading to an active, quenched, avalanche photo diode (APD) as the detector. As a result, the coherent factor β in dynamic laser light scattering was about 0.98. The avalanche photo diode has a sensitivity 2 orders higher than that of a normal photon multiplier (PM) tube, while its dark count increases no more than 10 times. Thus, a 22-mW laser could have a measured count rate similar to a 400 mW laser for a normal PM tube. For DLS experiments in this dissertation, the standard deviation of every measurement of hydrodynamic radius (R_h) can be automatically calculated and is below 1%. The schematic setup of the LLS is given in Figure 2.2.

Figure 2.1 A commercial ALV/DLS/SLS-5000 laser light scattering (LLS).

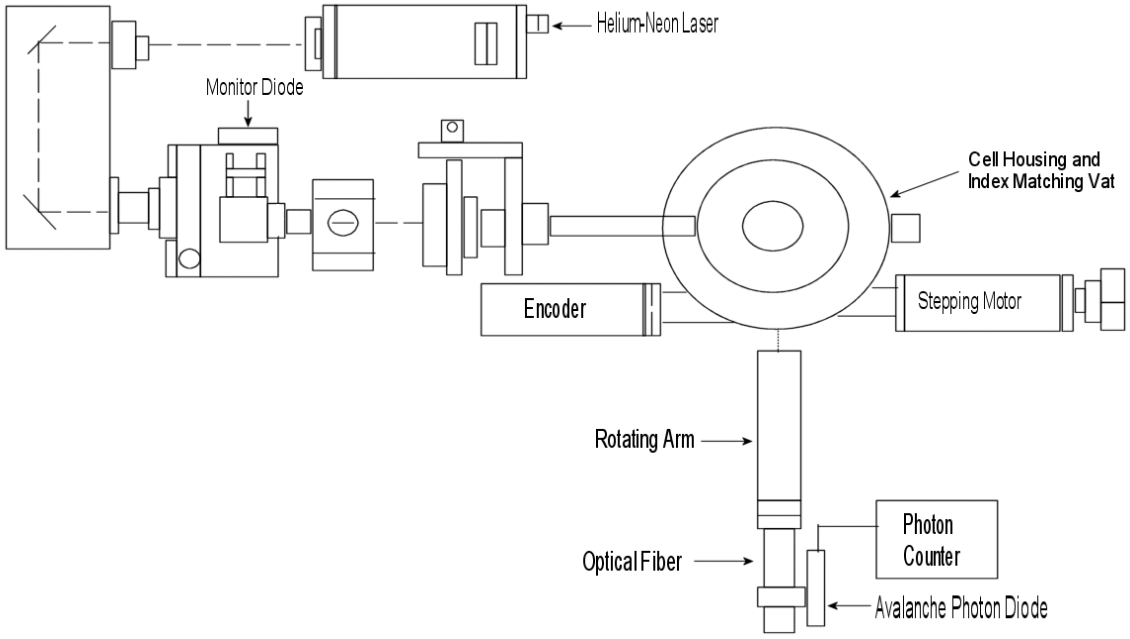

Figure 2.2 Schematic Setup of the Laser Light Scattering Instrument

REFERENCES

(1) Tanaka, T. *Experimental Methods in Polymer Science*; Academic Press, **2000**.

(2) Chu, B. *Laser Light Scattering*, 2nd edition; Academic Press, **1991**.

(3) Allcock, H. R.; Lampe, F. W. *Contemporary Polymer Chemistry*, 2nd edition; Prentice-Hall, Ins.: New Jersey, **1990**.

(4) Lu, X.; Hu, Z.; Gao, J. *Macromolecules* **2000**, *33*, 8698.

(5) Wu, C.; Chan, K. K.; Xia, K. Q. *Macromolecules* **1995**, *28*, 1032.

(6) Zhang, G.; Wu, C. *J. Am. Chem. Soc.* **2001**, *123*, 1376.

(7) Berne, B. J.; Pecora, R. *Dynamic Light Scattering*; John Wiley & Sons, Inc: New York, **1976**.

(8) Brown, W. *Dynamic Light Scattering*; Oxford University Press: Oxford, **1993**.

(9) Gao, J.; Haidar, G.; Lu, X. H.; Hu, Z. B. *Macromolecules* **2001**, *34*, 2242.

(10) Provencher, S. W. *Biophys. J.* **1976**, *16*, 29.

(11) Provencher S. W. *Makromol. Chem*. **1979**, *180*, 201.

CHAPTER 3

SYNTHESIS AND LIGHT SCATTERING STUDY OF HYDROXYPROPYL CELLULOSE MICROGELS[1]

3.1 INTRODUCTION

Microgels are crosslinked colloidal particles that can swell by the absorption of many times their weight of solvent and exhibit a behavior ranging from that of polymer solutions to that of hard spheres.[2-5] Treating a dispersion of identical colloidal particles as a one-component assembly of superatoms dispersed in a continuous background, microgel systems lead to the fundamental study of modeling the transition from liquid to crystal and from the supercooled liquid to the glassy state of atomic fluids.[5] From application point of view, the microgel particles can respond to environmental change much faster than bulk gels due to the much smaller size of the particles.[6] Unusual properties of microgels lead to various applications, including automotive surface coatings,[7] printing,[8] and controlled drug delivery.[9,10]

Many methods have been developed for preparing microgels, including emulsion polymerization,[11] inverse microemulsion polymerization,[12] anionic copolymerization,[13]and crosslinking of neighboring polymer chains.[14] Currently, thermally-responsive microgels as represented by N-isopropylacrylamide (NIPA), have attracted great attention due to their scientific importance and technological applications.[2] The important applications of NIPA include controlled drug release,

biosensor, and tissue engineering. The NIPA microgel was first synthesized by Pelton and Chibante in 1986.[11] In their study, the pre-gel solution of the NIPA monomer was heated above the lower critical solution temperature (LCST) of the NIPA polymer solution. The polymerization of the NIPA monomers and crosslinking polymer chains occurred simultaneously at the reaction temperatures above the LCST. Narrowly distributed NIPA microgel particles were obtained with their swelling properties similar to those of the bulk NIPA gel.[15]

In this chapter, we report synthesis and study of another important thermally responsive microgel -- hydroxypropyl cellulose (HPC). Bulk HPC hydrogel, including the homogeneous gel and the porous gel have been extensively studied before.[16,17] The HPC gel collapses and shrinks above the volume phase transition temperature T_c (~ 43°C), but swells and expands below T_c. In contrast to most synthetic gels that are made from carcinogenic or teratogenic monomers, the HPC gels, comprising natural cellulose ether macromolecules, have been approved by the United State Food and Drug Administration (FDA) and thus have significant practical advantages over the synthetic gels.[17] The chemical structure of the HPC is shown in Figure 3.1[18]

To our knowledge, however, synthesis of HPC microgels has not been reported. In contrast to previous work on the NIPA microgel that started from NIPA monomers, we demonstrated a process whereby HPC chains in a surfactant solution were heated above the LCST to give colloidal particles that were then crosslinked to form microgel particles. In this paper, our results will be divided into two parts. The first is to discuss synthesis of HPC microgels that involved fundamental interaction between high molecular weight

polymer chains and surfactant. The second is to discuss swelling properties and the volume phase transition of HPC microgel particles as a function of temperature, crosslinker concentration and quality of solvent. Light scattering techniques have been used for both monitoring microgel formation and characterizing the microgel particles. Such techniques have been widely used to study various microgels.[19,20]

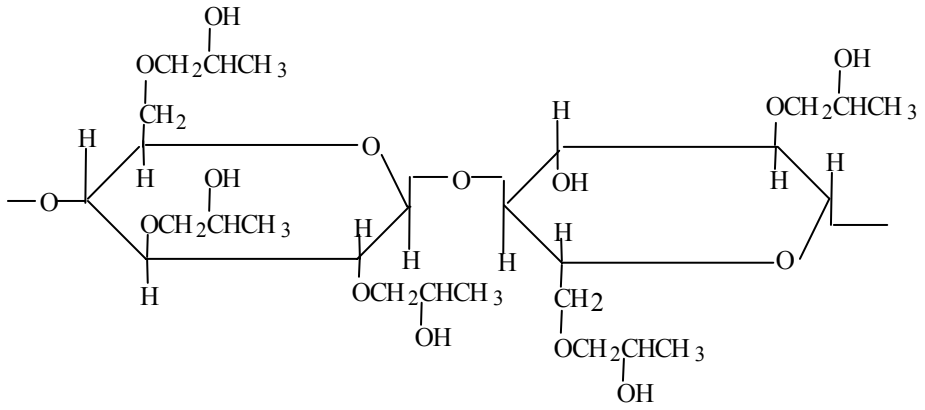

Figure 3.1. The chemical structure of the HPC polymer.

3.2 EXPERIMENTAL

Materials Dry hydroxypropyl cellulose(HPC) powder (average M_w =1x10^6), dodecyltrimethylammonium bromide (DTAB), divinyl sulfone (DVS), sodium hydroxide (NaOH) pellets and sodium chloride (NaCl) were purchased from Aldrich Chemical Company. The substitution level of the HPC polymer for this study was MS=3.9, where MS is the average number of molecules of propylene oxide combined per anhydroglucose unit. Deionized and distilled water was used throughout.

HPC Microgel Synthesis HPC hydrogel nanoparticles were synthesized using an emulsion method. 0.1wt% HPC aqueous solution was prepared as follows: 0.1 g HPC powder was dispersed in 99.9g aqueous sodium hydroxide solution (pH=12) by gentle stirring for a period of 4-6 days, until the HPC powder was thoroughly hydrolized. 0.475g of dodecyltrimethylammonium bromide (DTAB) was added to 100 g of 0.1wt% HPC solution and the solution was stirred for 60 minutes. Then 0.04g of crosslinker divinylsulfone (DVS), was added to the HPC solution. After mixing completely, the 0.1wt% HPC solution was heated up to about 55°C. Then the color of the HPC solution changed from clear to light blue, indicating the formation of nanoparticles. The reaction lasted for one hour at about 55°C. The resultant microgels were dialysized four times or more to remove the surfactant and NaOH. The same procedure was used to prepare the microgels in 0.15wt%, 0.2wt%, 0.3wt%, 0.4wt%, and 0.5wt% HPC solutions at different surfactant concentrations and at different reaction temperatures, respectively. The crosslinking mechanism is given as follows:[21]

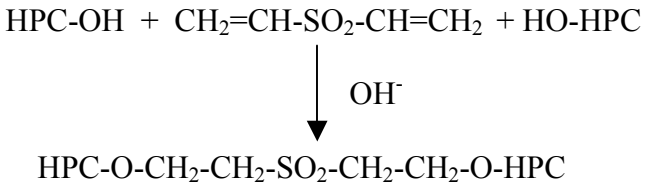

3.3 RESULTS AND DISCUSSION

A. Synthesis of HPC microgels

Table 3.1. Synthesis Condition, Average Radii <R_h>, and Polydispersity Index ($\mu_2 / \bar{\Gamma}^2$) of HPC Microgels

0.1 wt %HPC (ml)	DTAB (cmc*)	DVS (g)	reaction T (LCST, ^oC)	reaction time (h)	colloidally stable	<R_h> (nm)	$\mu_2 / \bar{\Gamma}^2$
100	1.0	0.04	55	1	yes	182	0.308
100	1.0	0.04	61	1	yes	179	0.204
100	1.0	0.04	64	1	yes	179	0.178

Note: The reaction occurred at the lower critical solution temperature (LCST) of 0.1 wt % HPC at various surfactant DTAB concentration. The cmc* is the critical micelle concentration, 1.54×10^{-2} mol/L, of surfactant DTAB in pure water at 25^0C.

The LCST of the 0.1wt% HPC solution increases with surfactant concentration as shown in Table 3.1. It is known that the pure HPC is more soluble in water at the temperatures below LCST (~41°C) than it is at the temperatures above the LCST.[16] This phase transition phenomenon may be explained by assuming that there are a number of equilibrium bond configurations for the propylene oxide moiety.[22-24] Each propylene oxide moiety in HPC comprises two C-O bonds and two C-C bonds. At low temperatures in polar solvents, oxygen atoms preferentially maintain a gauche orientation about the C-C bonds and a trans-configuration about the C-O bonds.[22-24] This particular bond conformation has a relatively large dipole moment. If the temperature is increased, or the solvating environment becomes less polar, then bond conformations that have a lower

dipolar moment may become more favorable. The dipole moment of the propylene oxide moieties may be reduced to such an extent that phase separation occurs.[22-24]

After introducing the cationic surfactant DTAB into nonionic HPC polymer in water, surfactant molecules self-assemble on the polymer chains, forming aggregates when a critical aggregation concentration is reached.[25] These aggregates are smaller in size than micelles. As more surfactant molecules accumulate on the HPC linear polymer, the micelles eventually form. When the surfactant concentration exceeds the CMC, which is the critical micelle concentration (1.54×10^{-2} mol/l) of DTAB in pure water at 25 ^{o}C, [26] the number of absorbed surfactant aggregates increases. The polymer chains attached with surfactant micelles become more hydrophilic due to the inter-aggregate electrostatic repulsion. As a result, the LCST of the HPC dispersion increases with surfactant concentration.

It is found that HPC polymer chains in a water-surfactant solution can collapse into colloidal particles at the LCST for DTAB surfactant concentrations ranging from 1 CMC to 1.5 CMC. Below 1 CMC, only very large particles (~10 μm) were observed. The collapsed polymer chains were stabilized by the charges on the surfactant micelles that are attached on the polymer chains. The collapsed HPC polymer chains in each colloid were chemically crosslinked by divinyl sulfone, and formed microgel particles.

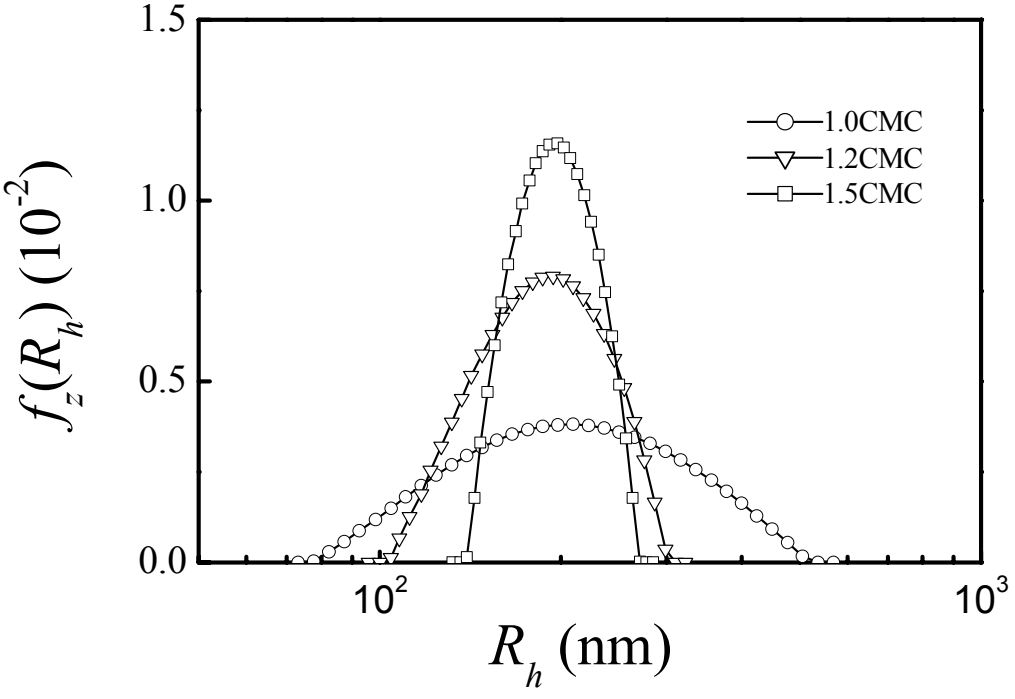

Figure 3.2. Hydrodynamic radius distributions ($f(R_h)$) of HPC microgel particles (C=8.94×10^{-6} g/ml) in deionized water at 25^{o}C. These particles were prepared in 0.1wt% HPC solution at various DTAB concentrations. Here the CMC is the critical micelle concentration of DTAB in pure water at 25°C and equals to 1.54 x 10^{-2} mol/l.

Figure 3.2 shows hydrodynamic radius distributions ($f(R_h)$) of HPC microgels (C=8.94×10^{-6} g/ml) in deionized water at 25^{o}C. These particles were prepared in 0.1wt% HPC solution with various DTAB concentrations at the LCST that corresponds to each DTAB concentration. In the surfactant concentration range studied, the average radii $<R_h>$ of the microgels were about the same. However, the radius distribution $f(R_h)$

becomes narrower with increasing surfactant concentration. This phenomenon could be due to the formation of more micelles in higher surfactant concentrations. The more charged micelles, the stronger electrostatic repulsion. This helps to stabilize the colloidal dispersion and make the particle size distribution narrower.

We also studied microgel formation as a function of HPC polymer concentration. In this experiment, the HPC concentration varied from 0.1 wt% to 0.3 wt%, while the DTAB concentration and the reaction temperature were fixed at 1 CMC and 55^{o}C, respectively. Figure 3.3 shows hydrodynamic radius distributions ($f(R_h)$) of HPC microgel particles (C= 8.94×10^{-6} g/ml) in de-ionized water at 25 ^{o}C. The average radius $< R_h >$ of the microgels becomes larger and its distribution becomes broader with the increase of HPC concentration. This result may be explained in terms of interaction of surfactant DTAB with HPC. As the HPC concentration increases, the average number of absorbed surfactant aggregates on each HPC polymer chain should decrease, reducing the inter-aggregate electrostatic repulsion force. This causes HPC linear chains to become more aggregated at higher HPC concentration. Thus, the average radius $<R_h>$ of the nanoparticles increases and its distribution becomes broader.

The reaction temperature plays an important role for the formation of the HPC microgel particles. Figure 3.4a shows hydrodynamic radius distributions ($f(R_h)$) of HPC microgel particles (C= 8.94×10^{-6} g/ml) in de-ionized water at 25^{o}C. These particles were

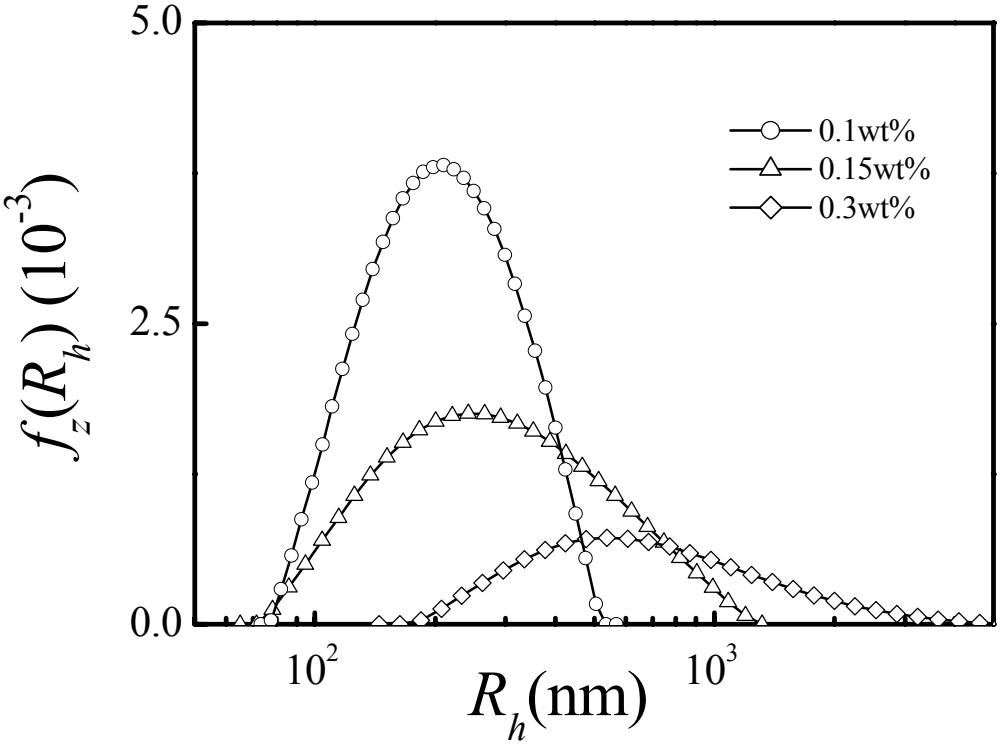

Figure 3.3. Hydrodynamic radius distributions ($f(R_h)$) of HPC microgel particles (C=8.94×10^{-6} g/ml) in deionized water at 25°C. These particles were prepared with various HPC concentrations at 1 CMC DTAB and at the reaction temperature 55^0C.

made at various reaction temperatures in 0.1wt% HPC solution and at 1 CMC DTAB concentration. The reaction temperature at which microgels formed is in a small range within about three degrees above the LCST, which is 55 °C for this dispersion. At each reaction temperature, experiments were repeated at least three times. The size distribution and average size of the HPC microgels are repeatable as shown in Figure 3.4b. Here,

reaction temperature was at 55^0C, and the measurements were performed at 25^0C in deionized water. Below the LCST, we did not observe formation of HPC nanoparticles. In this range studied, as the reaction temperature increases, the average radius of the resultant microgels becomes larger and the radius distribution becomes broader.

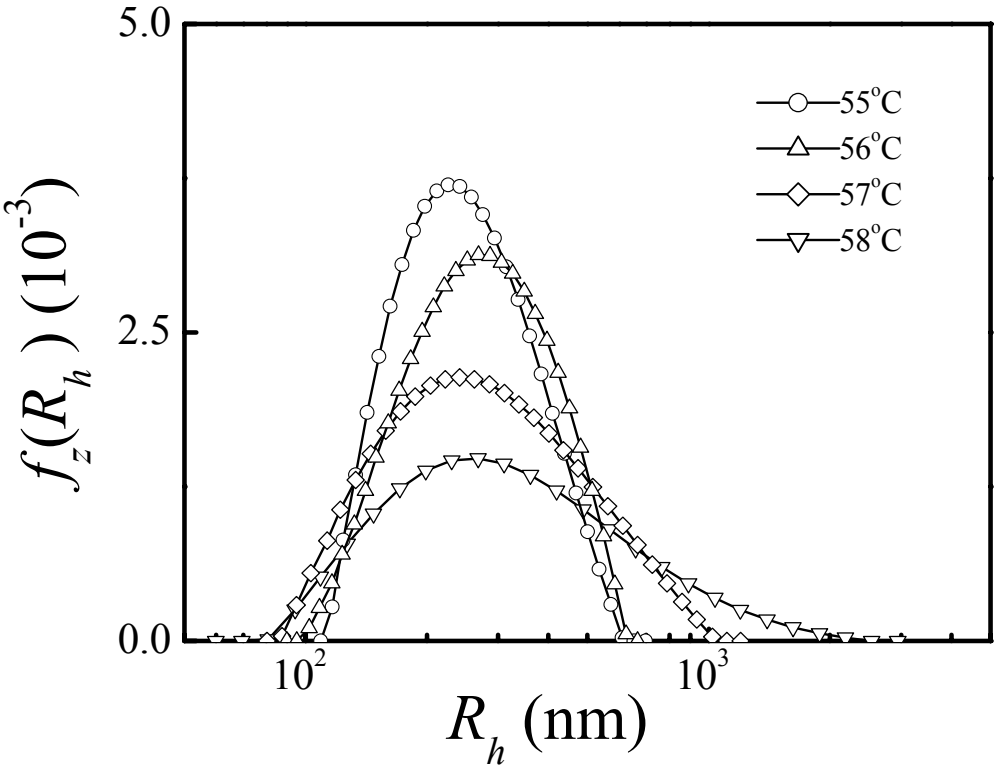

Figure 3.4a. Hydrodynamic radius distributions ($f(R_h)$) of HPC microgel particles (C= 8.94×10^{-6} g/ml) in de-ionized water at 25°C. These particles were made at various reaction temperatures in 0.1wt% HPC solution and at 1 CMC DTAB concentration.

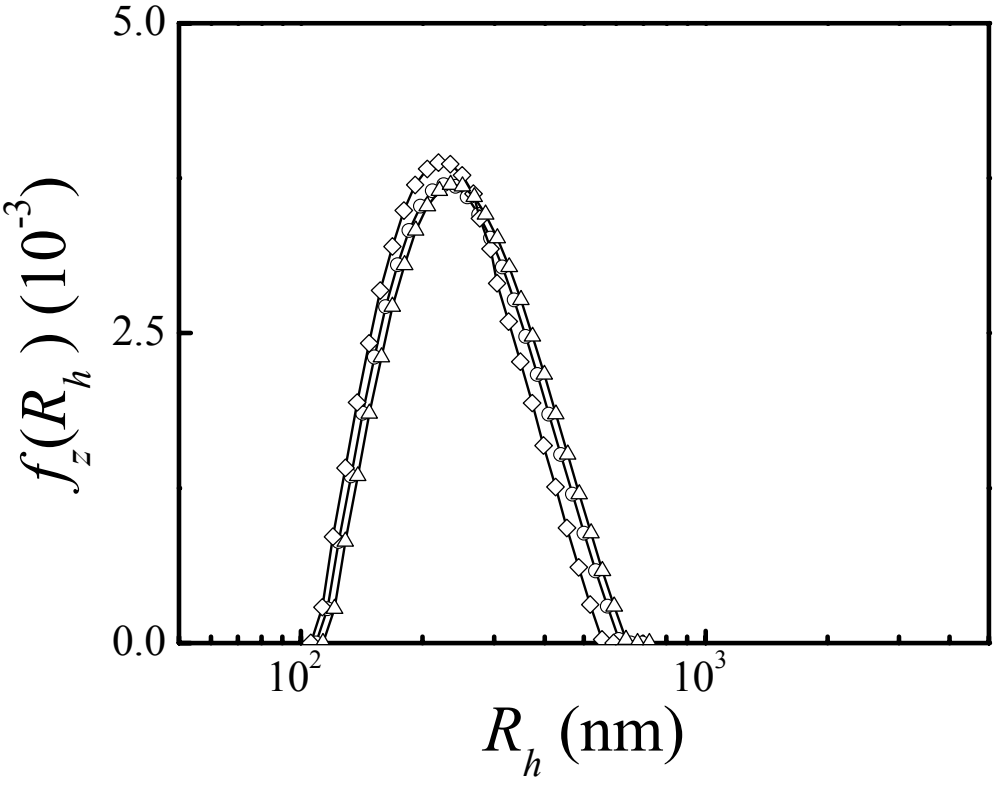

Figure 3.4b. Hydrodynamic radius distributions ($f(R_h)$) of HPC microgel particles (C= 8.94×10^{-6} g/ml) in de-ionized water at 25°C. These particles were made at 55^0C reaction temperature in 0.1wt% HPC solution and at 1 CMC DTAB concentration.

The reaction temperature-dependent size of the microgels is related to the HPC hydrophobicity and the interaction of surfactant with the HPC. As the reaction temperature just reached LCST, the aggregated HPC chains can form stable nanoparticles due to inter-micelle electrostatic repulsion. With the increase of reaction temperature above the LCST, the driving force for polymer-polymer aggregation increases. On the

other hand, the inter-particle electrostatic repulsion increases as particle size increases. As a result, more HPC chains aggregate to form larger particles until the new equilibrium between the hydrophobic interaction and inter-micelle electrostatic repulsion is reached.

B. Characterization of HPC microgels The swelling properties of HPC microgels were characterized using light scattering techniques after exhaustive dialysis to wash out surfactant and residual chemicals. The HPC microgels undergo a volume phase transition in water from a swollen state to a collapsed state as the temperature increases. The driving forces for the thermal-sensitive volume phase transition were considered to be a balance between the hydrophilic and hydrophobic interactions of inter- and intra-polymer chains.

We first discuss the volume phase transition of HPC microgels at various crosslinker concentrations. The volume phase transition temperature, T_c, is defined as the one that causes the sharpest rate of the change in gel volume. The average hydrodynamic radius plotted as a function of temperature is shown in Figure 3.5a. The volume phase transition temperature (T_c) was determined by taking a derivative of the R_h verse T curve. The peak location corresponds to T_c . As an example shown in Fig. 3.5 b, the volume phase transition temperature of the HPC microgels with 10 wt% crosslinking density is 41^0C. Although up to 20 wt% of crosslinker, relative to the HPC, is used during synthesis, solubility properties of the linear HPC polymer are expected to dominate the gel swelling behavior. The average molar mass of the segment between two neighboring crosslinking points, $\overline{M}_c$, is inversely proportional to the crosslinking concentration. As a result, the

degree of swelling at room temperature and the size change below and above T_c decrease with the increase of the crosslinking concentration. It is noted that the effective crosslinker concentration that actually contributes to the formation of the network is expected to be smaller than the one that was used in the polymerization process. This may be the main reason that the size contraction (about a factor 2 in Figure 3.5a) is quite large when one considers the fairly high degree of crosslinkers

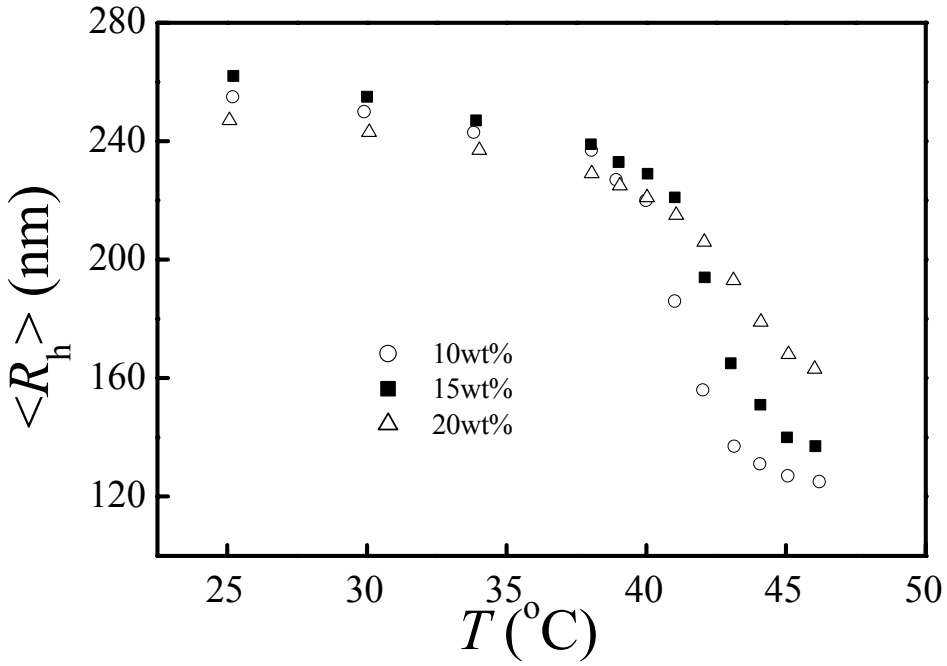

Figure 3.5a. The average hydrodynamic radius $\langle R_h \rangle$ of HPC microgel with different crosslinking density changes as a function of temperature in deionized water. The HPC microgels were prepared in 0.5 wt% HPC solution at 1.5 CMC DTAB and at the reaction temperature 65 ^{o}C. This same batch of microgels with 10 wt% crosslinking density was also used in Figures 3.6-3.8.

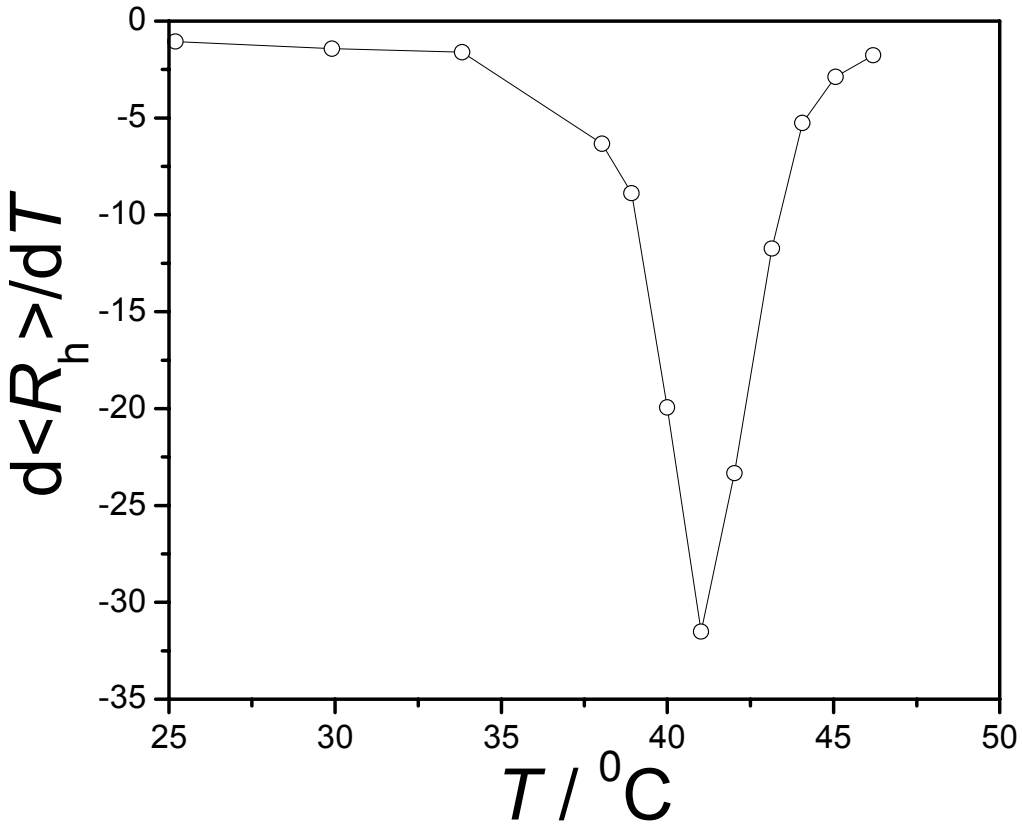

Figure 3.5b. Volume phase transition temperature of the HPC microgels with 10 wt% crosslinking density.

We also studied the size distribution of microgels below and above T_c. The plot of inverse of the time-averaged scattered intensity I^{-1} versus the square of wavevector, q^2, is shown in Figure 3.6 for the microgel dispersion of concentration 8.94×10^{-6} g/mL in water and the weight ratio of polymer to crosslinker of 10 wt%. The extrapolation of q^2 to

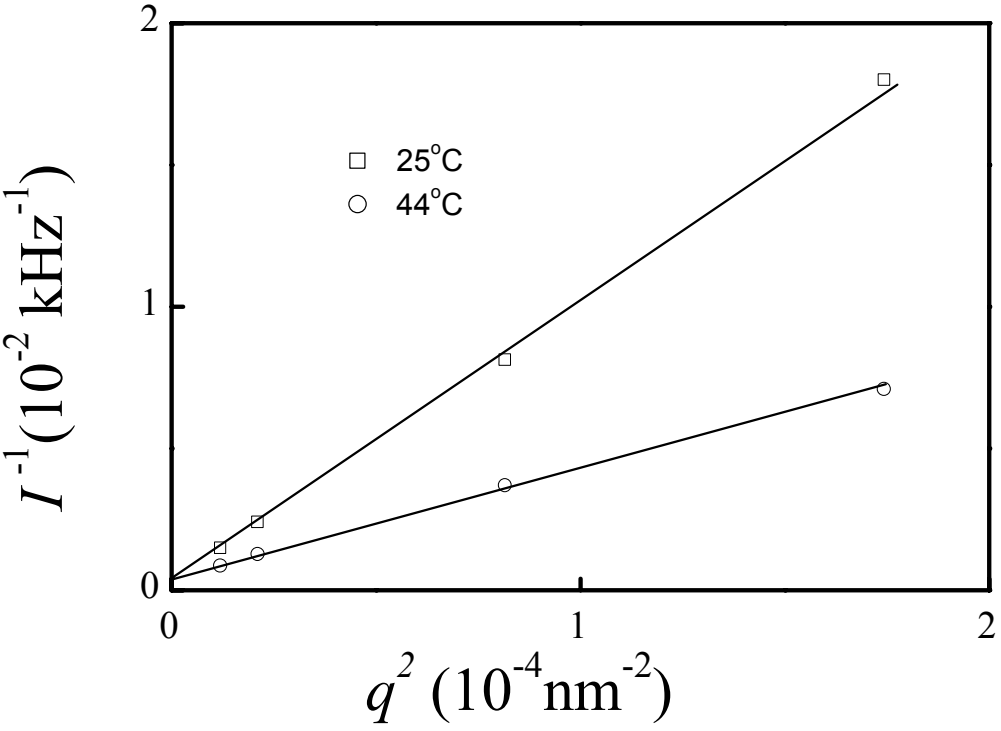

Figure 3.6. Inverse of time-averaged scattered intensity I^{-1} vs the wave vector square (q^2) of HPC microgel particles in de-ionized water at 25 ^{o}C and at 44 ^{o}C, respectively. The solid lines are the least square-fit to the data.

$q \rightarrow 0$ led to the same intercept at $\theta=0$. This indicates that the microgels are still stable at 44 ^{0}C, which is above T_c. It is noted that the HPC microgels have no electric charge on the surface, in contrast to the NIPA microgels. Although the NIPA polymer does not have charge, the NIPA microgel particles have charge, which are sulfate and carboxyl groups that originate from the ionic free radical polymerization initiator.[1] Thus,

stabilization of the HPC microgels at T> T_c is different from that of the NIPA microgels. The stability of the HPC microgel particles could be due to the steric interactions between these particles. The steric interaction produces the energy barrier to prevent microgels from aggregation at temperatures higher than T_c.[27]

Figure 3.7 shows the intensity auto-correlation functions and corresponding hydrodynamic radius distributions ($f(R_h)$) of the HPC microgels of concentration of 8.94×10^{-6} g/mL in de-ionized water at 25 ^{o}C and 44 ^{o}C, respectively. At 25 ^{o}C, the size distribution is very broad. This may be attributed to the relative broad length distribution of the tangling HPC chains on the particle surface. Since the crosslinking was directly performed on the long polymer chains that have an average molecular weight of about 1,000,000 , the variation of the length of the surface tangling chains could be quite large. As the microgels were heated above T_c, the loose surface tangling chains collapse, resulting in narrower particle size distribution.

The salt effect on the phase transition temperature of a dilute HPC microgel dispersion was also investigated. Figure 3.8 shows the average hydrodynamic radius $\langle R_h \rangle$ as a function of temperature for HPC microgel particles(C= 8.94×10^{-6} g/ml) in water and in 0.9 wt% NaCl solution (0.15mol.l^{-1}, physiological ionic strength), respectively. T_c is about 41 ^{o}C for the microgels in pure water, while it is about 39 ^{o}C for

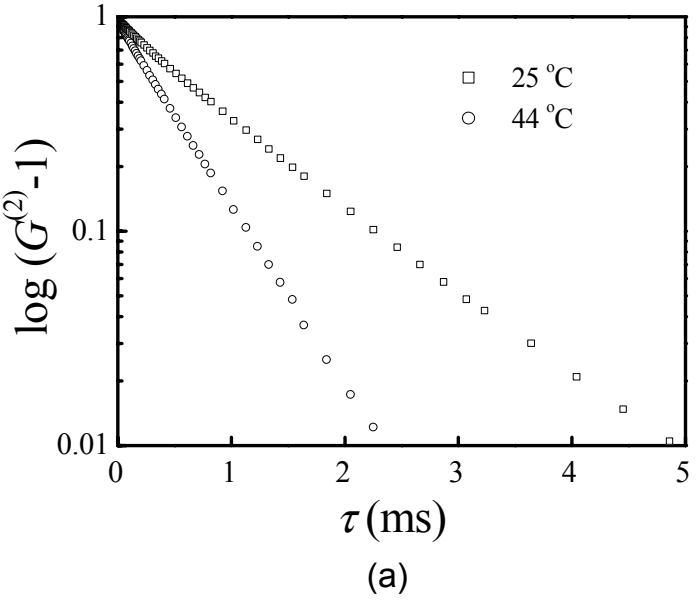

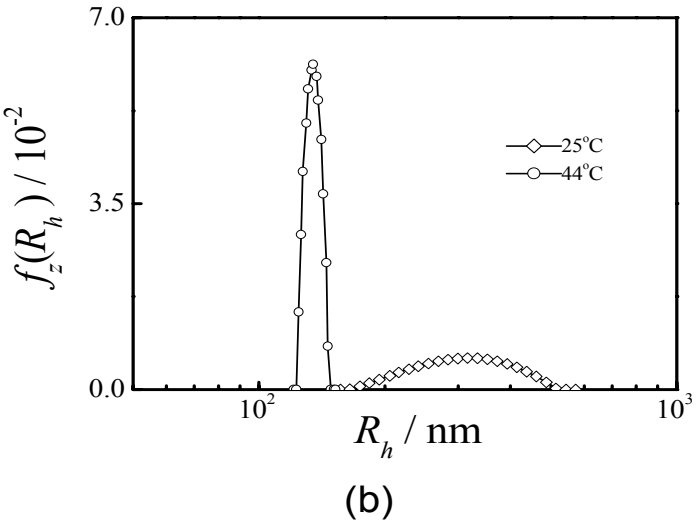

Figure 3.7. (a) Intensity autocorrelation functions of the HPC microgel in de-ionized water at 25 °C and 44 °C, respectively. (b) Corresponding hydrodynamic radius distributions ($f(R_h)$) of the samples.

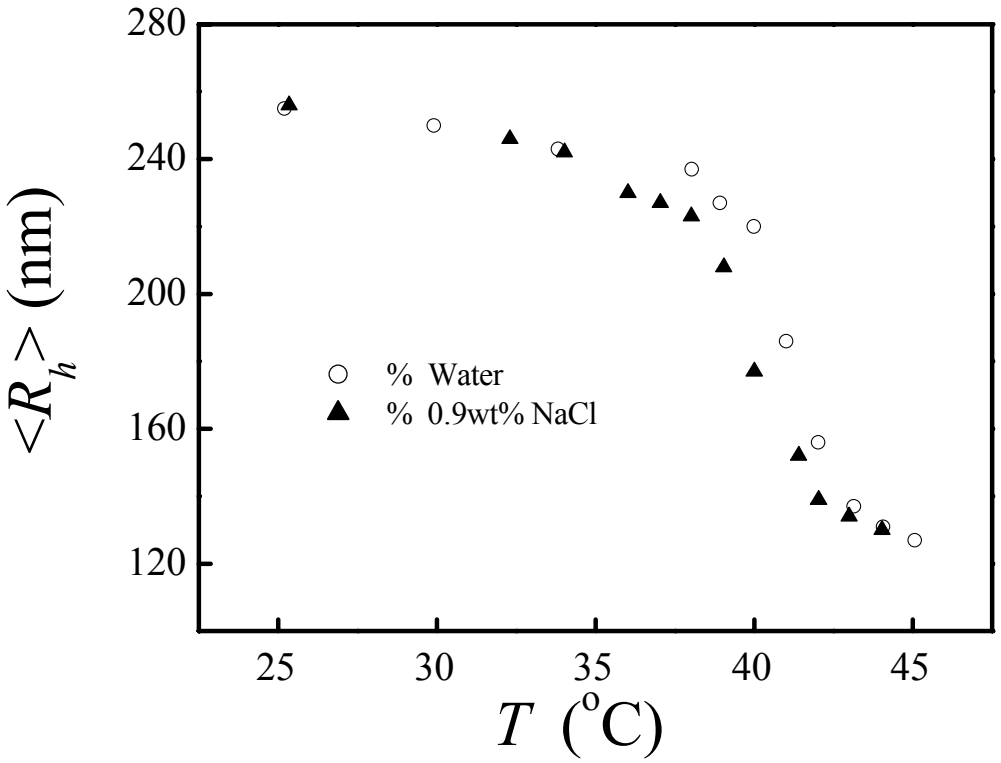

Figure 3.8. The average hydrodynamic radius $<R_h>$ of HPC microgels changes as a function of temperature in de-ionized water and in 0.9 wt% NaCl aqueous solution, respectively.

the microgel in 0.9 wt% NaCl. The decrease of T_c with the addition of NaCl may be because inorganic ions form hydrates through ion-dipole interactions.[28] The disturbance of water structure by adding NaCl in HPC dispersion induces contact between HPC polymer chains, causing the decrease of T_c of HPC microgels. Combining the

temperature-responsive volume change, the suitable transition temperature around 39 ^{o}C under the physiological condition that corresponds to the temperature as a person gets a fever, bio-compatibility of the HPC, and uniformed and small size, the HPC microgels could be particularly useful in controlled drug delivery applications.

3.4 CONCLUSION

HPC microgels have been synthesized for the first time by chemically crosslinking hydroxypropyl cellulose (HPC) linear macromolecules. The controllable synthesis parameters – surfactant concentration, HPC concentration and reaction temperature – were varied to determine the effects on the size and size distribution of the microgels as monitored using laser light scattering techniques. It is found that the microgels can form only above the CMC of the DTAB surfactant at the LCST. As the HPC concentration increases from 0.1 wt% to 0.3 wt%, the size distribution becomes significantly broader. Furthermore, the reaction temperature plays an important role for the size distribution: upon increase of the temperature above the LCST, the particle size increases quickly. The formation of microgels may be explained by the balance between the hydrophobic interaction between HPC polymer chains and inter-micelle electrostatic repulsion. The swelling and phase transition properties of the resultant HPC microgels are analyzed using both static and dynamic light scattering techniques as a function of temperature at various crosslinker concentrations. It is found that the increase in the crosslinker density reduces the shrinkage extent and increases the transition temperature. The dilute HPC microgel particles with a concentration of 8.94×10^{-6} g/ml form a stable colloidal

dispersion at room temperature and at 44^{o}C (>T_c), probably due to steric effects. In the aqueous solution of physiological salt concentration, the phase transition of the HPC microgels occur at about 39°C, which corresponds to fever temperature of human body. Combining the temperature-responsive volume change, bio-compatibility of the HPC, and uniform and small size, the HPC microgels could be particularly useful in controlled drug delivery applications.

REFERENCES

(1) Lu, X.; Hu, Z.; Gao, J. *Macromolecules* **2000**, *33*, 8698.

(2) Pelton, R. *Adv. Colloid Interf. Sci.* **2000**, *85*, 1.

(3) Saunders, B. R.; Vincent, B. *Adv. Colloid Interf. Sci.* **1999**, *80*, 1.

(4) Murry, M. J.; Snowden, M. J. *Adv. Colloid Interf. Sci.* **1995**, *54*, 73.

(5) Senff, H.; Richtering, W. *J. Chem. Phys.* **1999**, *111*, 1705.

(6) Li, Y.; Tanaka, T. *J. Chem. Phys.* **1990**, *40*, 820.

(7) Bradna, P.; Quadrat, Q.; Snuparck, *J. Colloid Polym. Sci.* **1995**, *273*, 324.

(8) Sasa, N.; Yamaoks, T. *Adv. Mater.* **1994**, *6*, 417.

(9) Sahoo, S. K.; De, T. K.; Ghosh, P. K.; Maitra, A. *J. Coll. Interf. Sci.* **1998**, *206*, 361.

(10) Kiser, P. F.; Wilson, G.; Needham, D.; *Nature* **1998,***394*, 459.

(11) Pelton, R.H.; Chibanate, P. *Colloids Surf.* **1986**, *120*, 247.

(12) Neyret, S.; Vincent, B. *Polymer* **1997**, *38*, 6129.

(13) Antionietti, M.; Pakula, T.; Bremser, W. *Macromolecules* **1995**, *28*, 4227.

(14) Frank, M.; Burchard, W. *Makromol. Chem. Rapid Commun.* **1991**, *12*, 64.

(15) Hirotsu, S.; Hirokawa, Y.; Tanaka, T. *J. Chem. Phys*. **1987**, *87*, 1392.

(16) Kabra, B. G.; Gehrke, S. H.; Spontak, R. J. *Macromolecules* **1998**, *31*, 2166.

(17) Harsh, D.C.; Gehrke, S. H. *J. Controlled Release* **1991**, *17*, 175.

(18) Winnik, F.M.; Tamai, N.; Yonezawa, J.; Nishimura, Y.; Yamazaki, I. *J. Phys. Chem.* **1992**, *96*, 1967.

(19) Wu, C. *Polymer* **1998**, *39*, 4609.

(20) Zhou, S; Chu, B. *J. Phys. Chem*. **1998**, *102*, 1364.

(21) Anbergen, U.; Oppermann, W. *Polymer* **1990**, *31*, 1854.

(22) Karlstrom, G.; Carlsson, A.; Lindman, B. *J. Phys.Chem.* **1990**, *94*, 5005.

(23) Ahlnas, T.; Karlstrom, G.; Lindman, B. *J. Phys. Chem.* **1987**, *91*, 4030.

(24) Karlstrom, G. *J. Phys. Chem.* **1985**, *89*, 4962.

(25) Hormnirun, P.; Sirivat, A.; Jamieson, A. M. *Polymer* **2000**, *41*, 2127.

(26) Drummond, C. J.; Albers, S.; Furlong, D. N. *Colloids Surf.* **1992**, *62*, 75.

(27) Lashkevich, O. V.; Dyagileva, A. B.; Chernoberezhskii, Y. M. *Colloid J.* **1997**, *59*, 467.

(28) Inomata, H.; Goto, S.; Otake, K.; Saito, S. *Langmuir* **1992**, *8*, 687.

CHAPTER 4

POLYMER GEL NANOPARTICLE NETWORK

4.1 INTRODUCTION

Polymer gels are a unique class of macromolecular networks that contain a large fraction of solvent within their structure. They are particularly suitable for biomedical applications because of their ability to simulate biological tissues.[1] In response to environmental stimuli such as temperature and pH, gels can reversibly swell or shrink up to 1000 times in volume[2] and have varied applications such as artificial muscles, controlled drug release, and sensors. [3-12] Gels are usually formed by the free radical polymerization of monomers in the presence of a difunctional crosslinking agent. They can be made either in bulk or in nano- or micro-particles. The bulk gels are easy to handle, but have a very slow swelling rate, while the gel nanoparticles act quickly to an external stimulus, but are too small for some applications. Here, by first making gel nanoparticles and then covalently bonding them together, we have engineered a new class of gels with two levels of structural hierarchy: the primary network is crosslinked polymer chains in each individual particle, while the secondary network is a system of crosslinked nanoparticles. Such nanostructured gels have new and unique properties that conventional gels do not have, including a high surface area, a bright blue color at room temperature, and temperature-tunable heterogeneity on the nanometer scale. This work may lead to creating opportunities for technological applications, ranging from controlled drug delivery, sensors, bio-adhesives, to displays.

4.2 EXPERIMENTAL

HPC Nanoparticle Synthesis The synthesis of the HPC nanoparticles was detailed in Chapter 3**.** 1 g of HPC (average molecular weight of $1x10^6$, Adrich Chemical Company) was dispersed to 200 ml of aqueous sodium hydroxide solution (pH=12). Divinylsulfone (DVS) (Sigma) of 0.1~0.5 ml per 1 g of HPC as a crosslinker and dodecyltrimethylammonium bromide of 1.425 g critical micelle concentration (c.m.c.) as a surfactant were then added to the HPC solution. The HPC nanoparticles formed within 1 hr at about 65 ^oC.

NIPA-co-AA Nanoparticle Synthesis 3.79 g NIPA monomer, 0.099 g AA monomer, 66 mg methylene-bis-acrylamide as crosslinker, 0.116 g sodium dodecyl sulphate as surfactant, and 240 mL deionized water were mixed in a reactor. The solution was heated to 70 ^oC under nitrogen for 40 min. 0.166 g of potassium persulfate dissolved in 21 mL of deionized water was added to start the reaction. The reaction was carried out at 70 ^oC for 4.5 h.

4.2 RESULTS AND DISCUSSION

As a demonstration, we first made hydroxypropyl cellulose (HPC) nanoparticles using an emulsion polymerization method. The nanoparticle dispersion was then dialyzed four times to remove surfactant and un-reacted chemicals. The average hydrodynamic radius ($<R_h>$) and R_h distribution function, $f(R_h)$ of these nanoparticles, were characterized using a commercial laser light scattering spectrometer (ALV/DLS/SLS-5000) with a Helium-Neon laser (Uniphase 1145P, output power of

22mW and wavelength of 632.8 nm). $\langle R_h \rangle$ ranged from 120 nm to 250 nm depending on chemical composition and reaction temperature. Crosslinking nanoparticles can be carried out either at room temperature or at the temperature above the volume phase transition temperature ($T_c \approx 41\ ^oC$)[13] of the HPC. When the reaction was set at T=55 ^oC ($>T_c$), 20 g of 0.5 wt% HPC nanoparticles were added into an aqueous sodium hydroxide solution of pH=12. After introducing divinylsulfone (DVS) of 0.02 ml, the residual hydroxyl groups on the surfaces of neighboring HPC nanoparticles were bonded to form a network. On the other hand, when the reaction was set at room temperature, the HPC nanoparticles did not precipitate. They were first closely packed to the concentration of 1.1 wt% using ultra-centrifugation and then crosslinked by adding DVS of 19.4 % in weight ratio of DVS to HPC at pH=12. The nanoparticle network was thoroughly washed in water. Since the nanoparticles were linked together by covalent bonding, they cannot be re-dispersed into solution, in contrast to well-known colloidal aggregates.

The gel nanoparticle networks prepared in this study have the water content ranging from 92 wt% to 97 wt%. It is noted that the crosslinkers can react not only with the functional groups of different nanoparticles but also with those of the same particles. Only inter-particle crosslinking contributes to the gel formation and the swelling and mechanical properties of the resulting materials.

Figure 4.1(a) and 4.1(b) show representative sketches of the HPC nanoparticle network, and the network of individual nanoparticle, respectively. The optical microscopic image of an HPC nanoparticle network in water at room temperature is

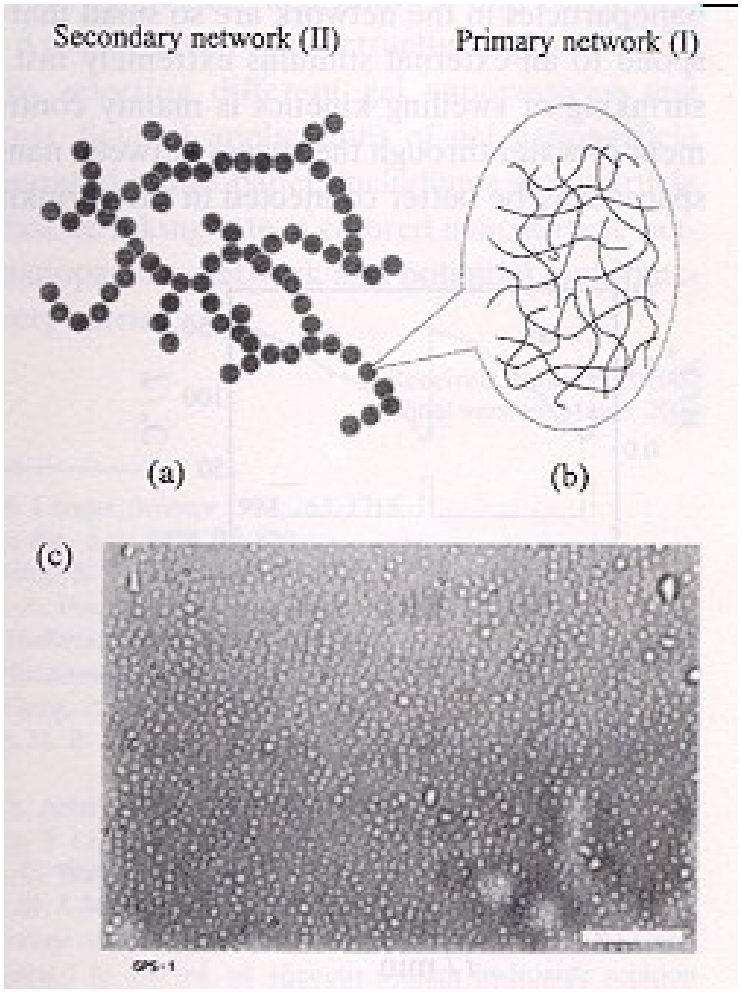

Figure 4.1. Structure of a polymer gel nanoparticle network. (a) Representative sketch of the gel nanoparticle network; (b) sketch of the gel network in each nanoparticle. The primary network (I) is crosslinked polymer chains in each individual nanoparticle, while the secondary network (II) is a system of crosslinked nanoparticles. (c) Optical microscopic image of the HPC nanoparticle network in water at room temperature. The network was formed at 55 ^{o}C. The white bar is 10 μm.

presented in Figure 4.1(c). As suggested in Figure 4.1(a) and 4.1(b), there are two different networks in a gel nanoparticle network. The primary network is crosslinked polymer chains inside each nanoparticle, while the secondary network is a crosslinked system of the nanoparticles themselves. The mesh size of the primary network depends on the concentration ratio of the crosslinker to linear polymer chains or monomers and is usually around 1-10 nm. In comparison, the mesh size of the secondary network depends on the concentration of the crosslinker and nanoparticles, and the size of nanoparticle. The mesh size is typically around 50-500 nm. As a result, the nanoparticle network could be used to entrap and deliver small or/and very large biomolecules with its primary and secondary structures, respectively. This will enhance the capability of polymer gels as carriers for controlled drug delivery.

The kinetics of volume change of polymer gels plays an important role for most of their applications ranging from sensors to actuators. Developing gel nanoparticle networks could drastically change such kinetics. As shown in Figure 4. 2, the swelling ratio of the HPC nanoparticle network with dimensions of 1 cm x 1 cm x 2.5 cm was measured as a function of time when the sample was cycled between two thermal baths set at 20 ^{o}C and 48 ^{o}C, respectively. This sample was synthesized using the same method as described above and crosslinking gel nanoparticles was controlled at room temperature. The HPC nanoparticle network swelled at 20 ^{o}C, but collapsed very quickly at 48 ^{o}C, which was above T_c. The HPC nanoparticle network exhibited distinctive asymmetric kinetics: its shrinking rate was faster by about two orders of magnitude than that of a conventional

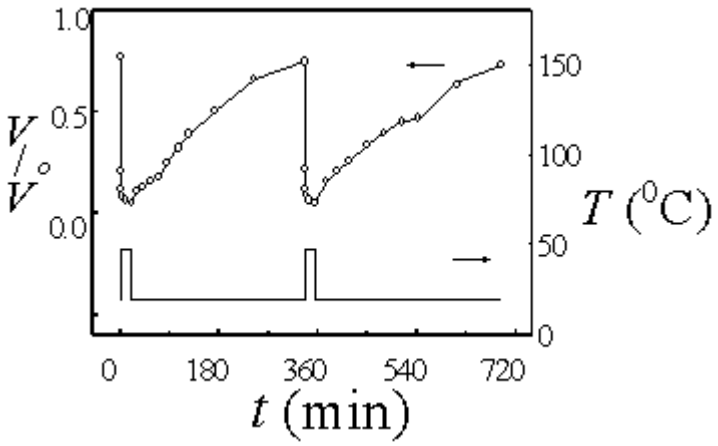

Figure 4.2. Swelling and shrinking kinetics of the HPC nanoparticle network that was formed at room temperature. Time-dependent swelling ratio of the sample that was cycled between two thermal baths set at 20 °C and 48 °C, respectively (open circles with the solid line). The temperature profile is represented using a solid line.

homogeneous gel with similar chemical composition and dimensions, while its swelling rate was not significantly higher.

The fast shrinking rate comes from the unique structure of the nanoparticle network. It is known that the shrinking or swelling time of a gel is dependent on the square of the smallest linear dimension, and is very slow for a bulk gel. [14] The nanoparticles in the network are so small that they should respond to an external stimulus extremely fast. Therefore, the shrinking or swelling kinetics is mainly controlled by movement of water through the spaces between nanoparticles. Such spaces may be better connected in the shrinking process than in the swelling process, resulting in the faster response rate in

shrinking. In comparison with other fast response gels that were made by either creating pores in the gel [15] or grafting hydrophobic chains into the gel,[16] the nanoparticle network has the advantages of highly uniform and easily tunable mesh sizes. For example, the pore size in a nanoparticle network can be well controlled by varying either nanoparticle size or the average number of nearest neighbors.

The nanoparticle networks can be made to retain some properties of their dispersions. As a demonstration, we first made nanoparticles of co-polymer N-isopropylacrylamide (NIPA, molar fraction of 96%) and acrylic acid (AA, 4%) using an emulsion method.[17] The NIPA has a thermally responsive property, while the AA provides carboxyl groups (-COOH) for crosslinking sites. The resulting NIPA-AA nanoparticles had an average radius of 153 nm at 25 ^{o}C in water as shown in Figure 4.3 (a). Upon exhaustive ultra-centrifugation, a concentrated NIPA-AA nanoparticle dispersion was obtained and it exhibited bright blue color. The color may be due to light interference from the closely packed nanoparticles. Epichlorohydrin was then added into the dispersion. The water in the naoparticles was gradually replaced by epichlorohydrin. After incubation at 98 ^{o}C for 10 h, crosslinking between epichlorohydrin and carboxyl groups occurred and the nanoparticles formed a network. This network was then transferred to acetone and finally to de-ionized water for thorough washing.

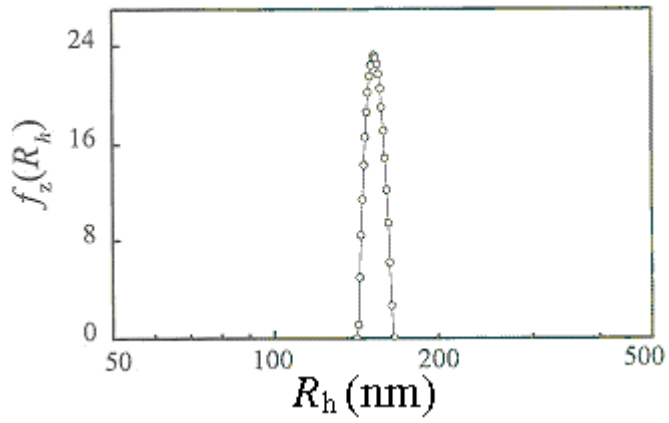

(a)

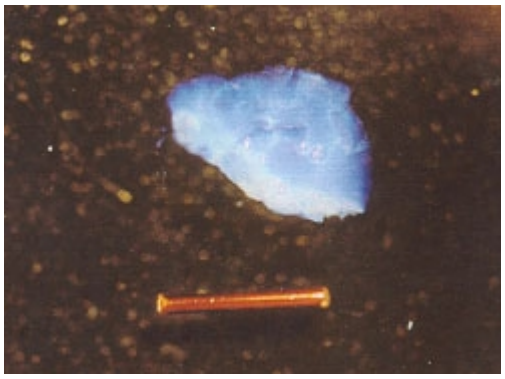

(b)

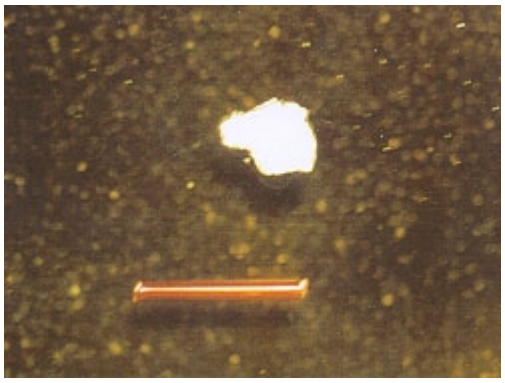

(c)

Figure 4.3. The NIPA-AA nanoparticles and its network with blue color. (a) Z-average hydrodynamic radius distribution of NIPA-AA nanoparticles at 25 ^{o}C in water. The nanoparticles as basic blocks were then crosslinked to form a network. (b) At 22 ^{o}C the network swelled and exhibited a blue color; (c) at 37 ^{o}C it shrank and exhibited a white color. The brown bar represents 1 cm.

This NIPA-AA nanoparticle network not only retained the blue color of the dispersion, but also had excellent mechanical stability that is lacking in conventional

dispersions. As shown in Figure 4.3 (b), the nanoparticle network kept its shape in water without support of a container at room temperature. When the temperature was increased to 37 ^{o}C (Figure 4.3 (c)), that is, above the volume phase transition temperature (T_c=34 ^{o}C) of the NIPA gel,[18] the network completely shrank and exhibited white color due to non-selective light scattering by microdomains formed during the volume transition.[19] Combining environmentally responsive color change and volume change, the nanoparticle network may potentially function as a display element or as a sensor for biological and medical applications.

It is expected that the nanoparticle network method could also be extended to stabilize crystal colloid arrays. The conventional colloid crystal arrays have found little practical application due to their poor mechanical and thermal stability.[20] To overcome this shortcoming, such arrays are usually embedded in a gel matrix.[9, 20] With our method, the colloidal crystal array could be stabilized by directly linking nanoparticles through chemical bonds without introducing another gel matrix.

Different nanoparticles can be used as basic building blocks for synthesis of co-nanoparticle networks. We demonstrated this idea by first synthesizing nanoparticles of poly(vinyl alcohol) (PVA) with radii about 125 nm and HPC with radii about 125 nm, respectively. The synthesis of HPC nanoparticles was mentioned above. The PVA nanoparticles were prepared using a surfactant-free method. PVA (88 mol% hydrolyzed, MW~25,000, Polysciences, Inc.) was dissolved in distilled water. Sodium hydroxide solution (5M) was added to yield 2 wt % PVA solution at pH=12. Then, 27 g of acetone was added to the 50 g PVA solution. After stirring 30 mins, 0.1 ml DVS was added to

the solution. The reaction lasted about four hours and the resulting nanoparticle dispersion was dialyzed five times. The PVA and HPC nanoparticles were then mixed. Crosslinking was performed by adding divinylsulfone to the PVA-HPC dispersion at pH=12 at 45 ^{o}C according to the following mechanism:

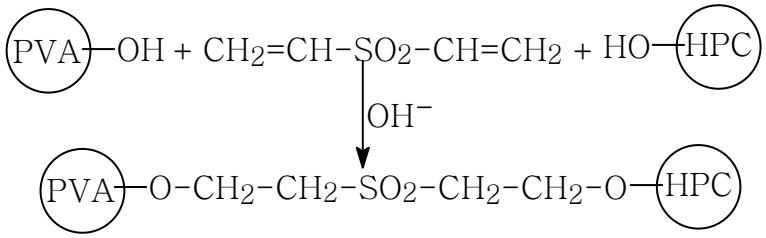

The PVA-HPC co-nanoparticle network was formed within 1 hour. In contrast to well-established co-polymerization with different monomers as building blocks, the co-nanoparticle network retains properties of each type of polymer nanoparticles. As a result, such a network could perform multifunctional tasks. For the PVA-HPC co-nanoparticle network, PVA nanoparticles could act as bioadhesive agents while the HPC particles act as drug carriers for temperature-controlled drug release. The bioadhesion of the PVA could be further improved because the surface area is greatly increased due to PVA nanoparticle structures. Furthermore, with an increase in the temperature, the PVA nanoparticles expand while the HPC nanoparticles shrink, resulting in temperature-tunable heterogeneity on the nanometer scale. The co-nanoparticle network technology may open a new avenue for synthesis of many new nanostructured polymeric materials.

4.4 CONCLUSION

In summary, a new class of nanostructured polymer gel has been synthesized by crosslinking gel nanoparticles through covalent bonds between functional groups on the surfaces of neighboring particles in solutions. Thus, these gels have two levels of structural hierarchy: the primary network is closslinked polymer chains in each nanoparticle, while the secondary network is crosslinked nanoparticles as a whole. With such a unique structure, they have new properties that conventional gels do not have, including high surface area, controlled heterogeneity at the nanoscale, and uniform and easily tunable mesh sizes. Architectures of nanostructured gels could be easily tailored by selecting different gel nanoparticles and crosslinking agents. Several applications of gel nanoparticle networks are presented in this chapter, including a nanoparticle network with a fast shrinking rate, a scattering-colored nanoparticle network, and a co-nanoparticle network as a potential multi-functional drug delivery carrier.

REFERENCES

(1) Peppas, N. A.; Langer, R. *Science* **1994,** *263*, 1715.

(2) Tanaka, T. *Phys. Rev. Lett*. **1978**, *40*, 820.

(3) Tanaka, T.; Nishio, I.; Sun, S. T.; Ueno-Nishio, S. *Science* **1982**, *218*, 467.

(4) Siegel, R. A.; Firestone, B. A. *Macromolecules* **1988**, *21*, 3254.

(5) Chen, G.; Hoffman, A. S. *Nature* **1995,** *373,* 49.

(6) Yoshida, R.; Takahashi, T.; Ichijo, H. *Adv. Mater*. **1997**, *9*, 175

(7) Osada, Y.; Gong, J. P. *Adv. Mater*. **1998**, *10,* 827.

(8) Weissman, J. M.; Sunkara, H. B.; Tse, A. S.; Asher, S. A. *Science* **1996**, *274,* 959.

(9) Holtz, J. H.; Asher, S. A. *Nature* **1997,** *389*, 829.

(10) Hu, Z.; Zhang, X.; Li, Y. *Science* **1995,** *269*, 525.

(11) Hu, Z.; Chen, Y.; Wang, C.; Zheng, Y.; Li, Y. *Nature* **1998**, *393*, 149.

(12) Snowden, M. J.; Murray, M. J.; Chowdry, B. Z. *Chemistry & Industry* **1996**, 531.

(13) Harsh, D. C.; Gehrke, S. H. *J. Controlled Release* **1991,** *17*, 175.

(14) Li, Y.; Tanaka, T. *J. Chem. Phys*. **1990,** *92,* 1365.

(15) Kabra, B. G.; Gehrke, S. H. *Polymer Comm*. **1991**, *32,* 322.

(16) Yoshida, R.; Uchida, K.; Kaneko, Y.; Sakal, K.; Kikuchi, A.; Sakurai, Y.; Okano, T. *Nature* **1995,** *374*, 240.

(17) Pelton, R. H.; Chibante, P. *Colloids Surf*. **1986,** *20*, 247.

(18) Hirotsu, S.; Hirokawa, Y.; Tanaka, T. *J. Chem. Phys*. **1987,** *87,* 1392.

(19) Li, Y.; Wang, G.; Hu, Z. *Macromolecules* **1995,** *28*, 4194.

(20) Kamenetzky, E. A.; Magliocco, L. G.; Panzer, H. P. *Science* **1994,** *263***,** 207.

CHAPTER 5

POLYMER HYDROGEL CRYSTALS

5.1 INTRODUCTION

Hydrogels have been studied extensively because of their abilities to simulate biological tissues[1, 2] and to swell or collapse reversibly in response to external stimuli.[3-11] They usually consist of a randomly crosslinked polymer chains and contain a large amount of water filling interstitial spaces of the network, resulting in amorphous structures. Without adding a coloring agent, the hydrogels are clear when they fully swell in water. Here we show a new class of bulk hydrogels with mesoscopical crystal structures. The central idea is to covalently bond self-assembled hydrogel nanoparticles. The covalent bonding contributes to the structural stability, while self-assembly provides them with crystal structures that diffract light, resulting in colors. As a result, these novel materials, which contain up to 97 wt % water, display a striking iridescence like precious opal but are soft and flexible like gelatin. This is in contrast to previous colored hydrogels, which were created either by adding dyes[12] or fluorescent molecules,[13] or organic solvents,[14] or by embedding a colloidal crystal array of polymer solid spheres.[15] In this chapter, three simple applications based on the crystal hydrogels are presented: a gel sensor with environmentally-tunable colors, a gel "opal" that displays a striking iridescence but is elastic and soft, and a gel display whose iridescent pattern can be made either visible or invisible by simply switching temperature. Creating such periodic 3D

structures in materials allows us to obtain useful functionality not only from the constituent building blocks, but also from the long-range ordering that characterizes these structures.[16]

5.2 EXPERIMENTAL

Two different building blocks of N-isopropylacrylamide (NIPA)-derivative nanoparticles, with various particle sizes, were synthesized using an emulsion polymerization method :[17,18] one was the NIPA co-polymerized with acrylic acid (AA)

Scheme 1

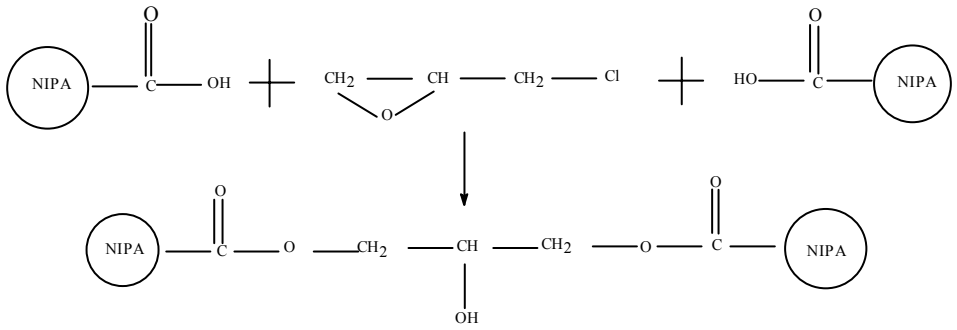

Scheme 2

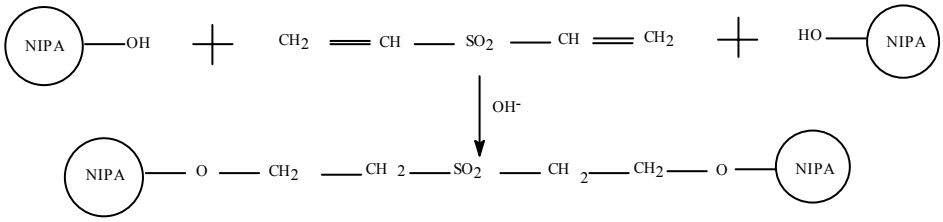

and the other was the NIPA with 2-hydroxyethyl acrylate (HEAc). The NIPA had thermally responsive properties ,[19] while the AA and the HEAc provided carboxyl (-COOH) and hydroxyl (-OH) groups, respectively, for the crosslinking sites. The size

distribution of nanoparticles was characterized using a light scattering spectrometer (ALV-5000). The hydrodynamic radius of the resultant nanoparticles in water was narrowly distributed with a size variance of about 1%.

We have developed two schemes for covalently bonding nanoparticle assemblies in either organic or aqueous media. In the first scheme, the NIPA-AA nanoparticles in water were first precipitated by adding acetone. These concentrated nanoparticles were transferred to a mixture of acetone/epichlorohydrin (1:3 volume ratio) to form a short-range-ordered structure by steric and electrostatic repulsion. After incubation at 98 ^{o}C for 10 h, the nanoparticles formed a three-dimensional network. This network was immersed in acetone and finally in de-ionized water for thorough washing. In the second scheme, the NIPA-HEAc nanoparticles first self-assembled into different structural arrays at various concentrations in an aqueous solution (pH=12). Then, divinylsulfone (DVS)[20] was added to bond them at room temperature. The second scheme can be carried out directly in water and is particularly useful for hydrogels. Since the colloidal particles are linked together by covalent bonding, they cannot be re-dispersed into a solution, in contrast to well-known colloidal aggregates. It is noted that the crosslinkers can react not only with the functional groups of different nanoparticles but also with those of the same particles.

5.3 RESULTS AND DISCUSSION

The NIPA nanoparticle assemblies exhibit phase behavior similar to conventional colloidal fluids discussed extensively elsewhere previousl.[21-23] These phase structures of

nanoparticles with an average hydrodynamic radius of 145 nm, have been stabilized using Scheme 2 as shown in Figure 5.1. In contrast to colloidal fluids, these assemblies are solids, and thus do not significantly deform due to gravity, as is apparent from the inverted orientation of the tubes. As shown in Figure 5.1(a), we found that it was difficult to bond the nanoparticles when the concentration was below 2.9 wt%, where the dispersions were in a liquid phase. In the concentration range 3.5 to 4.1 wt%, the assemblies exhibited iridescent color patterns, indicating that the nanoparticles self-assembled into a macro-crystal phase of long-range order. The crystal grain size decreased with increasing concentration. When the concentration was above 5 wt%, the crystals were too small to be observed, and the nanoparticles self-assembled into a glass phase of short-range order. The color of the assemblies, for a fixed particle size, became bluer because the scattering wavelength becomes shorter with increasing nanoparticle concentration . On the other hand, as the particle size increased, the color shifted to the red and the crystal phase occurred at a lower concentration (Figure 5.1(b)).

To quantify these observations, we have measured the turbidity of NIPA nanoparticle dispersions as a function of the wavelength as shown in Figure 5. 2 (a) using a spectrophotometer.[24] Similar techniques have been used to study colloidal silica in poly(methyl acrylate) film.[25, 26] Corresponding to the appearance of colors, the turbidity of the dispersions exhibited a shoulder-shaped increase as the wavelength decreased.

a

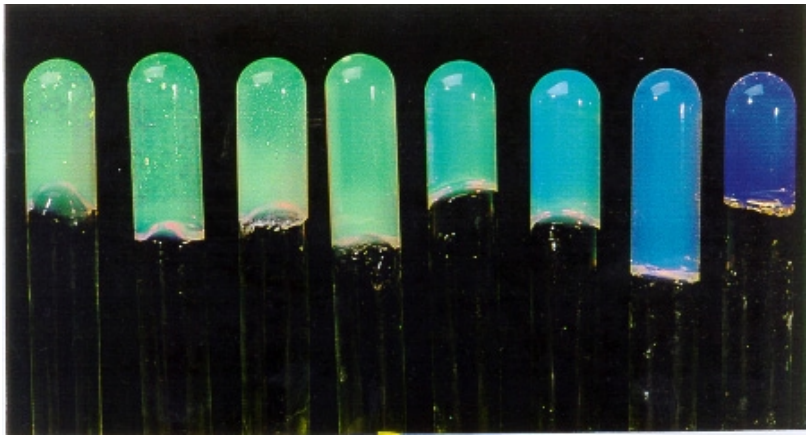

b

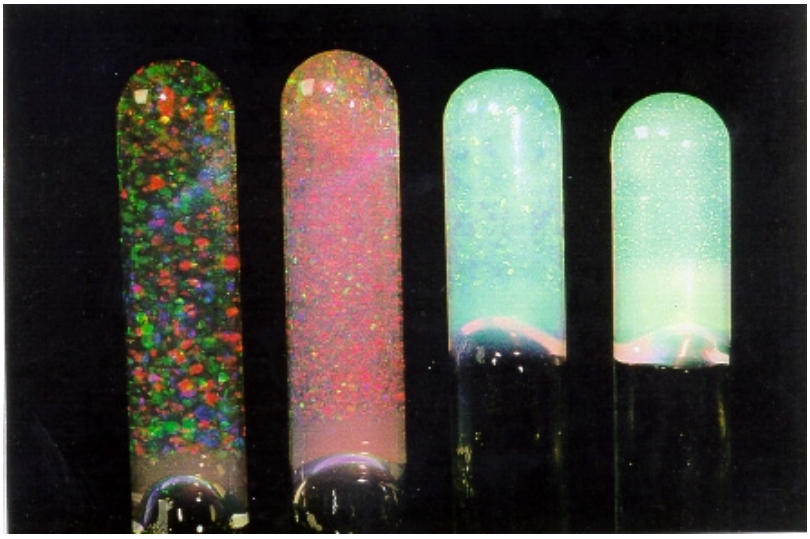

Figure 5.1. The covalently bonded, self-assembled NIPA nanoparticles made with Scheme 2. (a) Photographs of samples at various particle concentrations. From left to right: 3.5, 3.8, 3.9, 4.1, 5.0, 5.5, 6.0, and 7.9 wt%. Here, the average hydrodynamic radius of the NIPA nanoparticle spheres in water at 25 ^{o}C was 145 nm. (b) Highlights of the crystal phase. The average hydrodynamic radii for the two red samples (left) and the two green samples (right) in water at room temperature were 175 and 145 nm, respectively. From left to right, the particle concentrations were 3.0, 3.1, 3.8, and 4.0wt%

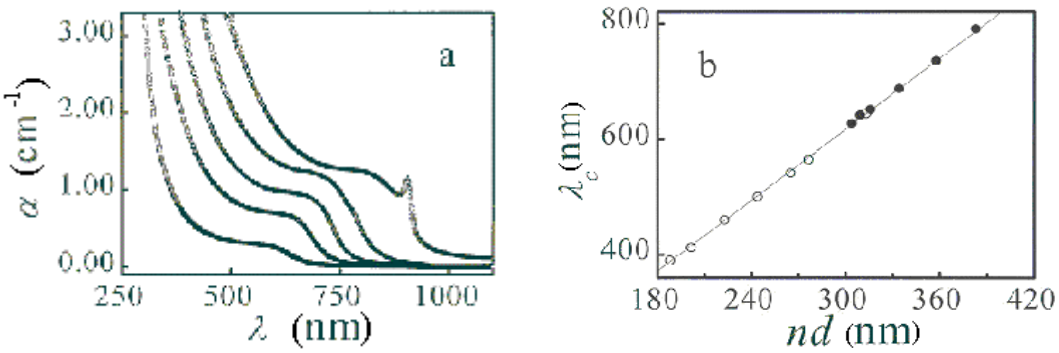

Figure 5.2. Optical properties of self-assembled NIPA nanoparticles. (a) The turbidity is plotted as a function of wavelength for NIPA nanoparticle arrays in water at various concentrations. The polymer concentrations for the curves from the right to left were 4.47, 6.78, 8.38, 10.4, and 14.2 wt%, respectively. The nanoparticles in water at 25 ^{o}C had an average hydrodynamic radius of 216 nm. (b) Linear relationship between the inter-particle light distance nd and λ_c, at which the turbidity exhibited a shoulder-shaped increase with decreasing wavelength. Two batches of samples with different radii were measured: solid circles represent R_h = 216 nm, and open circles represent R_h = 132 nm. The line represents the least-square fit of λ_c (nm) = 2.04nd + 4.1, where n is the refractive index of the nanoparticles.

Let us define λ_c as the transition wavelength at the position of the half height of the shoulder. λ_c is linearly proportional to the interparticle distance (d) as shown in Figure 5.2 (b) for two batches of the nanoparticles that had average hydrodynamic radii of 132 nm and 216 nm, respectively. D is calculated assuming nanoparticles form either the face-centered cubic lattice[27] or the hexagonal close-packed lattice with the packing

fraction of 0.74. A least-square fit yields λ_c (nm) = 2.04nd + 4.1, indicating that the Bragg diffraction condition of $2nd\sin\theta = m\lambda_c$ is satisfied with the diffraction angle $\theta = 90°$ and m = 1. Here n is the refractive index of hydrogel nanoparticles. For $\lambda > \lambda_c$, the Bragg diffraction condition can never be satisfied, while for $\lambda < \lambda_c$, it can be satisfied by polycrystals with different orientations of $\theta < 90^o$. The colors of the samples arise from selective Bragg diffraction at $\lambda < \lambda_c$. Because the inter-particle distance can be adjusted by varying either concentration or particle size, the colors of the samples can be shifted accordingly.

Figure 5.3(a) shows a typical NIPA nano-structured hydrogel that was made using Scheme 1 and that was immersed in acetone. A uniform and intense green color indicates that it has retained the short-range order of its colloidal precursor. Color changes were observed either when the sample was transferred from acetone to water at 21 ^oC or when the sample was warmed from 21 ^oC to 31 ^oC in water (Figure 5.3(b)). Conventional gel sensors based on volume phase transitions require a large size change from a swollen state to a collapsed state, which is usually discontinuous and nonlinear. [28] In contrast, the current systems based on distance between nanoparticles require only small size changes that can be linearly correlated to the color as suggested by Figure 5.2b. The color of the hydrogel could be further tuned by applying an electric field of 3.5V/cm in deionized water at room temperature as shown in Figure 5. 3(c). The electric field caused electrolysis in the water solvent and an ion gradient that resulted in gel volume change.[29] This effect was not observed when the electrodes were placed outside the insulating container holding the gel and its solvent while applying an electric field of 3.5 V/cm.

a 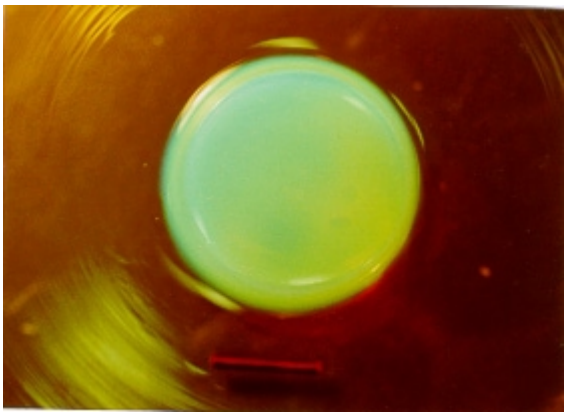

.

b 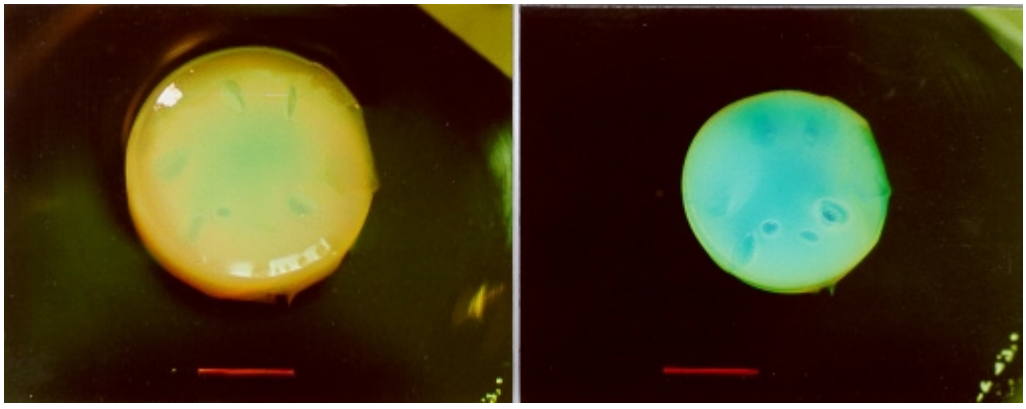

c 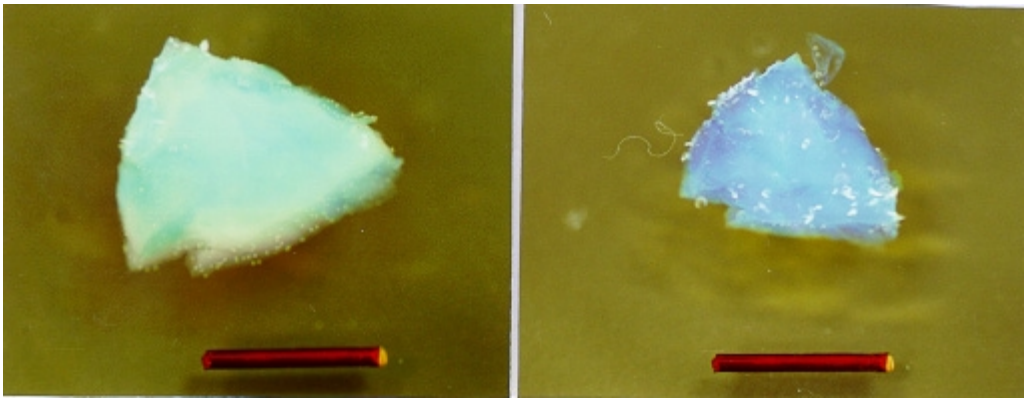

Figure 5.3. Environmentally responsive color and shape changes of bonded NIPA nanoparticle assemblies. All samples were made with Scheme 1. The bar represents 1 cm. (a) A fully swollen gel nanoparticle network in acetone. (b) The same sample in water at 21 ^{o}C (left) and 31 ^{o}C (right). (c) The color of a sample (left) in water at room temperature changed as an electric field of 3.5V/cm was applied to it (right).

Using Scheme 2, we synthesized a gel "opal" immersed in a pH=2.5 solution at room temperature as shown in the top panel of Figure 5. 4(a). The iridescent pattern of the sample is a clear indication that the sample has retained the crystal structure of its colloidal precursor. After applying a weight (a transparent dish) on the sample's upper surface, the sample was compressed (the bottom panel, Figure 5.4(a)) and deformed greatly. The fractional increases in length were 80% along the radial direction and 40% along the longitudinal direction. Once the weight was removed, however, the network immediately returned to its original shape due to its elasticity and re-exhibited the iridescent pattern, as shown in the top panel. It is noted that iridescent colors are usually

associated with rigid materials such as precious opal [30] that can deform slightly, or with colloidal fluids[31] that have no definite shape. Here, we have created a soft material that is elastic, wet, and exhibits an iridescent pattern.

The covalent linkages between nanoparticles also lead to the remarkable thermal stability of the crystal structure. Figure 5.4 (b) shows the temperature dependence of a crystal hydrogel in a tube after polymerization with Scheme 2. The iridescent pattern (left panel) at room temperature became invisible when the sample was heated to 50 ^{o}C, at which point the gel became cloudy due to phase separation (right panel). When the sample at 50 ^{o}C was cooled back to 21 ^{o}C, the pattern reappeared within 10 s, and this process was reversible. In contrast, a non-crosslinked nanoparticle assembly with the same concentration was completely disrupted as the temperature was raised to 32 ^{o}C. It required about 1000 times longer for a non-crosslinked assembly to re-assemble into a crystal structure. It is apparent that disturbed nanoparticles in a crosslinked assembly are able to return to their equilibrium crystalline positions quickly through restoring forces provided by the network elasticity. The fast response rate of the crystal hydrogels could be a major advantage for developing sensor or display technologies over conventional colloidal crystal arrays.

It is noted from the left panel in Figure 5.4(b) that the crystal hydrogel in water displays an iridescent color with good transparency and no sedimentation (without adding an index-matching or a density-matching fluid). This is because the building blocks are hydrogel nanoparticles which contain up to 97 wt% water; both the refractive index and the density of the particles are nearly matched with those of the surrounding water. The

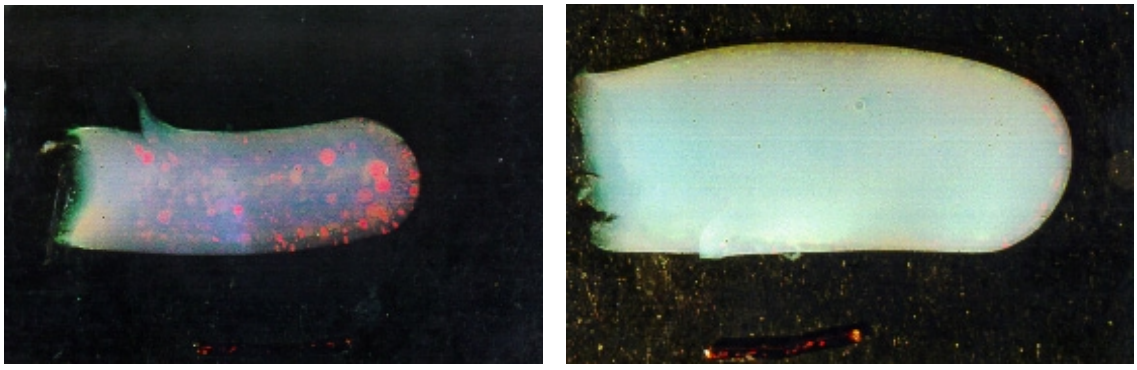

(a)

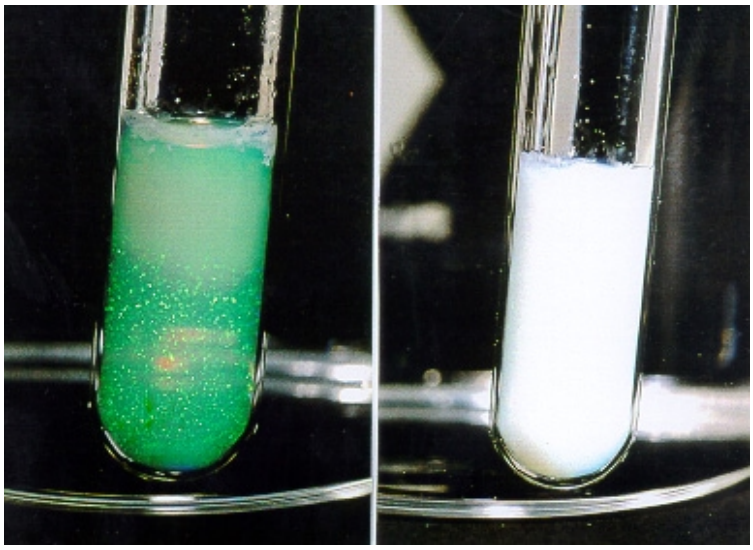

(b)

Figure 5.4. The NIPA crystal hydrogels made with Scheme 2. (a) A hydrogel "opal". The sample was placed in a pH=2.5 solution before (top) and after (bottom) applying a weight (a transparent dish) to compress it. The bar represents 1.165 cm. (b) A crystal hydrogel display. The sample in the tube is transparent and exhibited an iridescent pattern at 21 ^{o}C (left) until the temperature was raised to 50 ^{o}C (right), at which point the pattern became invisible. As the sample at 50 ^{o}C was cooled back to 21 ^{o}C, the patterns reappeared within 10 s.

crystal structures of our systems are further enriched by their unique two-level structural hierarchy:[32] The primary network consists of crosslinked polymer chains inside each nanoparticle, while the secondary network is a crosslinked system of the nanoparticles. The mesh sizes of the primary and the secondary networks are approximately 1-10 nm and 10-500 nm respectively.

5.4 CONCLUSION

In summary, hydrogel opals have been synthesized by covalently bonding self-assembled hydrogel nanoparticles. The covalent bonding contributes to the mechanical and thermal stability of the assemblies, while self-assembly provides the bulk hydrogels with crystal structures which diffract light, resulting in colors. Several applications of crystal hydrogels are presented in this chapter, including a gel sensor whose color can be tuned by either temperature or an electric field, a gel "opal" that displays a striking iridescence and is wet and elastic, and a gel display whose iridescent pattern can be made either visible or invisible by simply switching temperature. This work may lead to technological applications, ranging from sensors and displays to home decoration.

REFERENCES

(1) Peppas, N. A. *Hydrogels in Medicine and Pharmacy,* (CRC Press, Boca Raton, FL, **1987**).

(2) Peppas, N. A.; Langer, R. *Science* **1994,** *263*, 1715.

(3) Tanaka, T. *Phys. Rev. Lett*. **1978**, *40*, 820.

(4) Tanaka, T.; Nishio, I.; Sun, S. T.; Ueno-Nishio, S. *Science* **1982**, *218*, 467.

(5) Siegel, R. A.; Firestone, B. A. *Macromolecules* **1988***, 21*, 3254.

(6) Osada, Y.; Okuzaki, H.; Hori, H. *Nature* **1992**, *355*, 242.

(7) Chen, G.; Hoffman, A. S. *Nature* **1995,** *373*, 49.

(8) Beebe, D. J.; Moore, J. S.; Bauer, J. M.; Yu, Q.; Liu, R. H.; Devadoss, C.; Jo, B. H. *Nature* **2000,** *404***,** 588.

(9) Yoshida, R.; Takahashi, T.; Ichijo, H. *Adv. Mater.* **1997**, *9*, 175.

(10) Y. Osada, and J. P. Gong, *Adv. Mater.* **1998**, *10,* 827.

(11) Snowden, M. J.; Murray, M. J.; Chowdry, B. Z. *Chem. Ind.* **1996**, 531.

(12) Hu, Z.; Zhang, X.; Li, Y. *Science* **1995***, 269*, 525.

(13) Oya, T.; Enoki, T.; Grosberg, A. Y.; Masamune, S.; Sakiyama, T.; Takeoka, Y.; Tanaka, K.; Wang, G.; Lilmaz, Y.; Feld, M. S.; Dasari, R.;Tanaka, T. *Science* **1999**, *286*, 1543.

(14) Gong, J. P.; Okuzaki, H.; Osada, Y.; *Macromol. Chem. Phys*. **1994**, *195*, 1871.

(15) Weissman, J. M.; Sunkara, H. B.; Tse, A. S.; S. A. Asher, *Science* **1996**, *274*, 959; Holtz, H.; Asher, S. A.; *Nature* **1997**, *389*, 829.

(16) Xia, Y.; Gates, B.; Yin, Y.; Lu, Y. *Adv. Mater*. **2000**, *12*, 693; Xia, Y. *Adv. Mater*. **2001**, *13*, 369.

(17) Pelton, R. H.; Chibante, P. *Colloids and Surfaces* **1986**, *20*, 247.

(18) 3.78 g NIPA monomer, 0.099 g AA monomer, 66 mg methylene-bis-acrylamide as crosslinker, 0.106 g sodium dodecyl sulphate as surfactant, and 240 mL deionized water were mixed in a reactor. Acrylic acid (AA) (4% molar ratio) or 2-hydroxyethyl acrylate (HEAc) (9.5% molar ratio) as functional groups were added to the pregel solutions, respectively. The solution was heated to 70 ^{o}C under nitrogen for 40 min. 0.166 g of potassium persulfate dissolved in 21 mL of deionized water was added to start the reaction. The reaction was carried out at 70 ^{o}C for 4.5 h.

(19) Hirotsu, S.; Hirokawa, Y.; Tanaka, T.; *J. Chem. Phys*. **1987**, *87*, 1392.

(20) Harsh, D. C.; Gehrke, S. H. *J. Controlled Release* **1991**, *17*, 175.

(21) Clark, N. A.; A. J. Hurd, A. J.; Ackerson, B. J. *Nature* **1979**, *281*, 57.

(22) Pusey, P. N.; van Megen, B. *Nature* **1986**, *320*, 340.

(23) Senff, H.; Richtering, W. *J. Chem. Phys*. **1999**, *111*, 1705.

(24) It is noted that the systems used for the turbidity study were neutral NIPA gel nanoparticle dispersions. The concentration ranges for

occurrence of various phases were slightly different from those of ionic NIPA gel nanoparticles that were used for the formation of nanopaticle networks in Schemes 1 and 2. However, the optical properties for both systems should be the same.

(25) Jethmalani, J. M.; Sunkara, H. B.; Ford, W. T.; Willoughby, S. L.; Ackerson, B. J. *Langmuir* **1997**, *13*, 2633 and references cited therein.

(26) Jethmalani, J. M.; Ford, W. T.; Beaucage, G. *Langmuir*, **1997**, *13*, 3338.

(27) Hellweg, T.; Dewhurst, C. D.; Bruckner, E.; Kratz, K.; Eimer, W. *Colloid Polym Sci.* **2000**, *278*, 972.

(28) Schild, H. G. *Prog. Polym. Sci*. **1992**, *17*, 163.

(29) Hirotsu, S. *Japn. J. Appl. Phys*. **1985**, *24*, 396.

(30) Sanders, J. V. *Nature* **1964**, *204*, 1151.

(31) Krieger, I. M.; O'Neill, F. M. *J. Amer. Chem. Soc.* **1968**, *90*, 3115.

(32) Hu, Z.; Lu, X.; Gao, J. Wang, C. *Advanced Materials* **2000**, *12*, 1173.

CHAPTER 6

PHASE TRANSITION BEHAVIOR OF HYDROXYPROPYL CELLULOSE UNDER INTERPOLYMER COMPLEXATION WITH POLY(ACRYLIC ACID)

6.1 INTRODUCTION

Interpolymer complexes are physically interacted polymer chains in solution and have been extensively investigated.[1-4] The formation of polymer complexes between a proton-accepting polymer such as poly(ethylene oxide) (PEO) and a proton-donating polymer such as poly(acrylic acid) (PAA) v*ia* H-bonding in aqueous media has attracted a continuing interest as a model of biological systems.[5-9] The complexation of different polymers in solution is a commonly used procedure for tailoring polymer properties to specific needs without chemical modification of these macromolecules. Most studies have been performed on the polymer complex systems, mainly focusing on the factors that affect complexation, including stoichiometric ratio of two complementary polymers, pH, ionic strength, solvent, concentration, and structure of the component polymers. [10-12]

However, only a few studies[13-14] have been reported so far on the effect of complexation on the low critical solution temperature (LCST) of a nonionic polymer, that is the minimum point at which phase separation will invariably occur in a polymer solution. Hence, for a model study, we have chosen the hydroxypropyl cellulose (HPC) as a proton-accepting polymer and poly(acrylic acid) (PAA) as a proton-donating

polymer to study how the complexation (Figure 1) between these two polymers affect the LCST of the HPC polymer under various conditions.

The HPC exhibits a lower critical solution temperature (LCST) at 41 ^{0}C and remarkable hydration-dehydration changes in aqueous solution in response to relatively small changes in temperate around the LCST.[15] Below the LCST, the HPC chains hydrate to form an expanded structure; above the LCST, the HPC chains dehydrate to form a shrunken structure. This property is due to the reversible formation and cleavage of the hydrogen bonds between the HPC and surrounding water molecules with changing temperature. The swelling behavior of HPC bulk gels, microgels, and polymer chains have been previously reported.[15-17] The advantage of HPC over many other synthetic thermally responsive macromolecules is that the HPC is one of the cellulose ethers approved by the United States Food and Drug Administration for the use in food, drug and cosmetics,[18-20] whereas many synthetic macromolecules are produced from carcinogenic and teratogenic monomers.

It is well known that incorporating hydrophobic comonomers leads to a lower LCST,[21] and incorporating hydrophilic comonomers leads to a higher LCST.[22] The changes in LCST caused by incorporating comonomers are due to changes in the overall hydrophilic properties of the polymer. This effect has been investigated for another important thermally responsive polymer N-isopropylacrylamide (NIPA).[21, 22]

Here we will show that based on complexation between the HPC and the PAA, the LCST of the HPC can be drastically changed. Our literature survey shows that studies of the structure and properties of interpolymer complexes between poly(acrylic acid) and

nonionic cellulose ethers have been reported.[23-31] Specifically, Budtova[23-26] and coworkers investigated the formation and properties of the interpolymer complexation between PAA and cellulose ethers including hydroxyethylcellulose (HEC) and methylcellulose (MC). Their experimental results showed that the mixtures of the cellulose ethers and non-ionized PAA in aqueous solution formed interpolymer complexes due to hydrogen bonding. However, to our knowledge, systematic studies of the phase transition behavior of the HPC/PAA complex with change of pH have not been reported. In this chapter, the results of phase transition behavior of HPC/PAA complex in water will be given, studied by turbidity and dynamic laser light scattering measurements as functions of polymer concentration, temperature, pH value, and macromolecular weight.

The complexation between the HPC and the PAA also leads to a new method for the formation of surfactant-free PAA nanoparticles directly in aqueous media at room temperature. Such microgels have very narrow size distributions as characterized by light scattering techniques and can reversibly swell and shrink in response to external stimuli such as pH. These microgels may be used as building blocks for the formation of nanoparticle networks[32] or carriers for controlled drug delivery.

6.2 EXPERIMENTAL

Materials. Dry hydroxypropyl cellulose (HPC) powder (average $M_w = 1.0\times10^6$, and average $M_w = 1.0\times10^5$), and poly(acrylic acid) (PAA) solution (25% wt., average M_w = 2.4 x 10^5; 25% wt., average $M_w = 9.0\times10^4$; 25%) was purchased from Aldrich Chemical Co. Deionized and distilled water was used throughout.

Sample Preparation. HPC powder was dissolved in dionized water by gentle stirring for three to four days at a concentration of 1 wt %. Also, the 25 wt % solution of PAA was diluted to 2.5 wt %. These two solutions were then mixed to produce the desired concentrations studied in this paper. For different pH solutions, phosphate buffered saline and 10 mM acrylic acid buffers were employed.

Turbidity Measurement. The increased insoluable polymer concentration can absorb light and reduce the transmission of visible light. This reduction can be measured and is called the sample's turbidity. Turbidity can be thought of as a sample's cloudiness.

The turbidity, a, will be defined as the reduction in light intensity per unit penetration length in the sample: $a = -(1/I)(\partial I/\partial x)$, where I is the light intensity in the sample. In the calculation, we can set L to be the path length or the thickness of the sample, I_t to be the intensity of the transmitted light, I_0 to be the intensity of the incident light, and set aL equal to constant, and then say that

$$I_t / I_0 = e^{-a L}$$

Therefore, the turbidity can be found from the percent transmittance or $a = - (1/L) \ln(I_t/I_0)$.[33]

In our experiment, we chose the wavelength of the incident light to be 555 nm. The absorbance was monitored using a spectrophotometer (Milton Roy Ltd. Spectronic 301) and the temperature of the sample was controlled by a circulation water bath (Fisher Scientific, Model 9110), accurate to 0.05^o C. The temperature of the sample was actually measured using a digital multimeter and a thermocouple configuration standardized at 0^o

C with ice. The sample was allowed thirty minutes or longer to reach equilibrium after each temperature adjustment.

6.3 RESULTS AND DISCUSSION

Effect of polymer concentrations and molecular weight on the LCST of HPC-PAA complex Hydroxypropyl cellulose in water has the LCST at 41^0C,[15] while poly(acrylic acid) is a hydrophilic macromolecule and readily dissolve in water. When the HPC and the PAA are mixed, the interpolymer complex is formed at pH<pK_a (pK_a =4.7 for acrylic acid[34]) due to hydrogen bonding between the HPC and the PAA as shown in Figure 6.1. That is, the PAA polymers act as a proton donor interacting with a proton acceptor (HPC) to form interpolymer complexes.

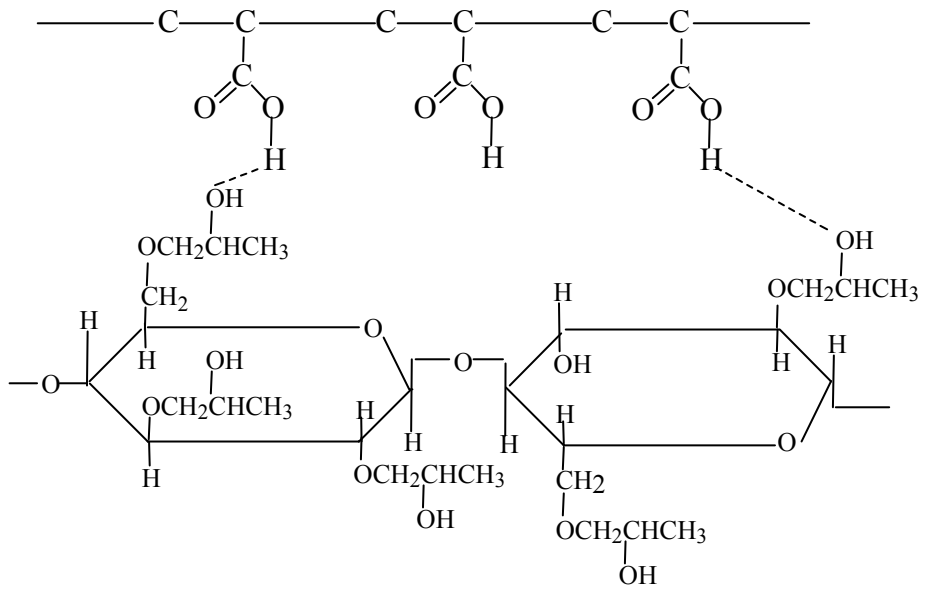

Figure 6.1 . Schematic hydrogen bonding between HPC and PAA[31]

Figure 6.2a shows the turbidity of the HPC-PAA complex in aqueous solution as a function of temperature at different HPC concentrations (average M_w = 1 x 10^6) at pH=3.2. The LCST of the HPC shifted to a lower temperature upon increasing HPC concentration from 0.15 to 0.60 wt% while the PAA is at 1.0 wt %, compared to that of pure HPC solution. The decrease of the phase transition temperature is contributed to the formation of inter-macromolecular chain complexes caused by hydrogen bonding between the –COOH group of PAA and –OH group of HPC. The formation of hydrogen bonds between the –COOH and –OH groups limits the accessibility of water to the HPC chains, leading to an increase in the hydrophobicity of the HPC linear macromolecules. This means that the solvating microenvironment for the complex system becomes less polar. As a result, the dipole moment of the propylene oxide moieties of HPC linear macromolecules may be reduced to such an extent that the phase transition occurs at much lower temperature.[35] Furthermore, for different HPC concentrations, there is a slightly slower LCST in 0.6 wt % than in other two samples. This could be due to stronger hydrophobic interaction in higher HPC concentration.

To study the effect of molecular weight on the LCST of the HPC-PAA complex, the turbidity as a function of temperature was measured for lower HPC molecular weight M_w=1.0x10^5 at pH=3.2. Figure 6.2b showed that the LCSTs of the HPC with lower molecular weight are higher than those of the HPC with higher molecular weight at the

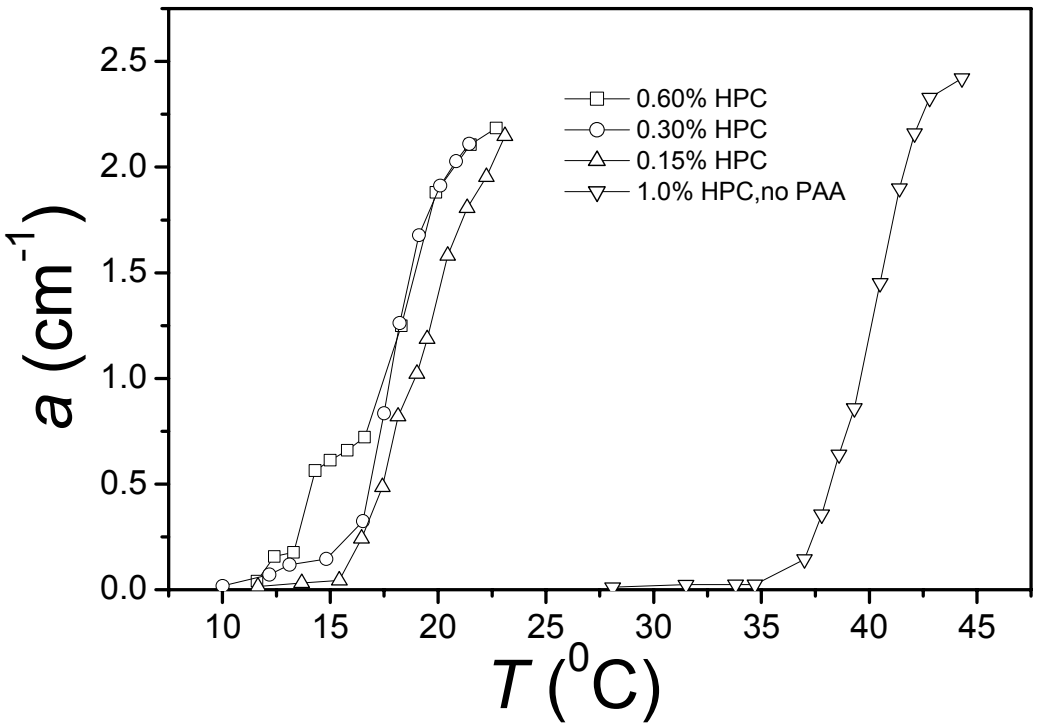

Figure 6.2a. The turbidity of the HPC/PAA for different HPC concentrations of $M_w=1.0\times10^6$ at PAA concentration $C_{PAA}=1.0$wt% at pH=3.2.

same polymer concentrations. This phenomena could be due to weaker intermolecular hydrogen bonding interaction for lower molecular weight HPC. The HPC chains of higher molecular weight are more easily removed from the aqueous environment and have the lower phase transition temperature. Two complexes with lower HPC concentrations in Figure 6.2b almost showed the same onset of the phase transition. The different HPC concentrations seem only to widen the temperature-response range of the complex and to change the magnitude of turbidity.

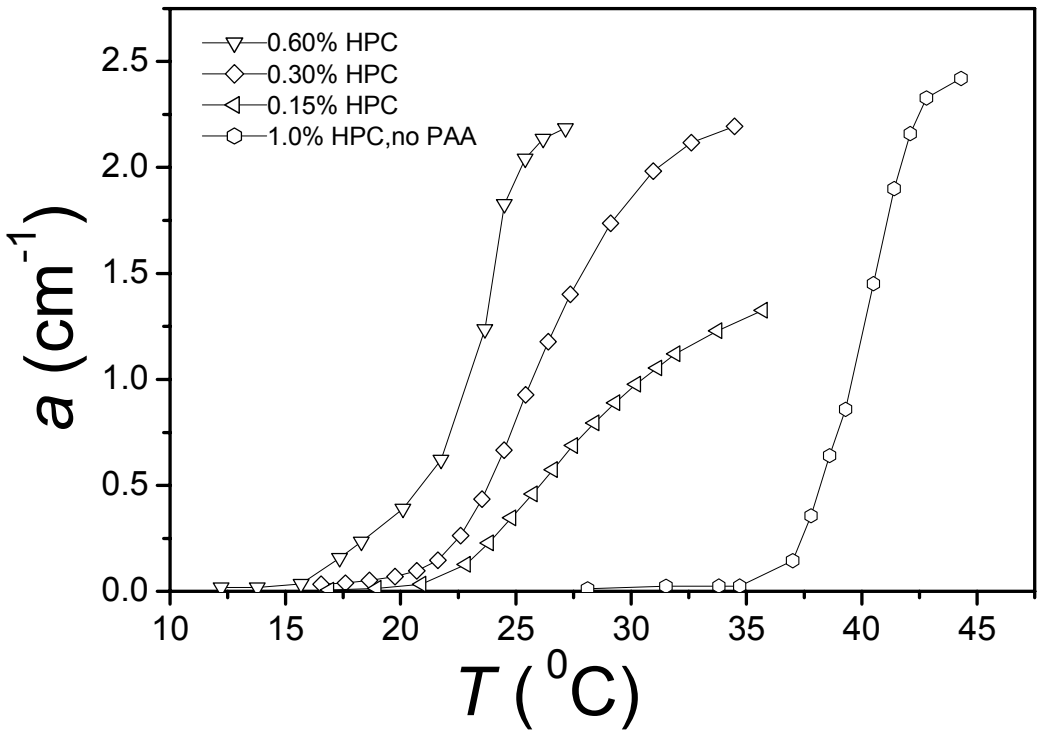

Figure 6.2b. The turbidity of the HPC/PAA for different HPC concentrations of M_w=1.0×10^5 at 1.0wt% PAA concentration at pH=3.2.

Previous work has shown that the macromolecular weight of the interacting polymer plays a very important role in forming the complexes.[4] Specifically, Morawetz[36-37]et al studied the effect of molecular weight of proton-accepting polymers on the complexation of PAA with polyvinylpyrrolidone (PVP) or poly(ethylene oxide) (PEO) using fluorescence spectroscopy. They found that the interaction of inter-macromolecular hydrogen bonding became stronger with the increase of the molecular

weights of the proton-accepting polymers. The same mechanism may cause the decrease of the LCST of HPC-PAA complex upon increasing the HPC molecular weight.

As a further study, we measured the turbidity of 1.3 wt% complexes with two different PAA molecular weights for 1 wt% PAA and 0.3wt% HPC ($M_w = 1.0\times10^6$) at pH=3.2. It was found that the molecular weight of the totally hydrophilic polymer PAA also affects the LCST of the complexes. The higher the PAA molecular weight, the lower the LCST, as expected.

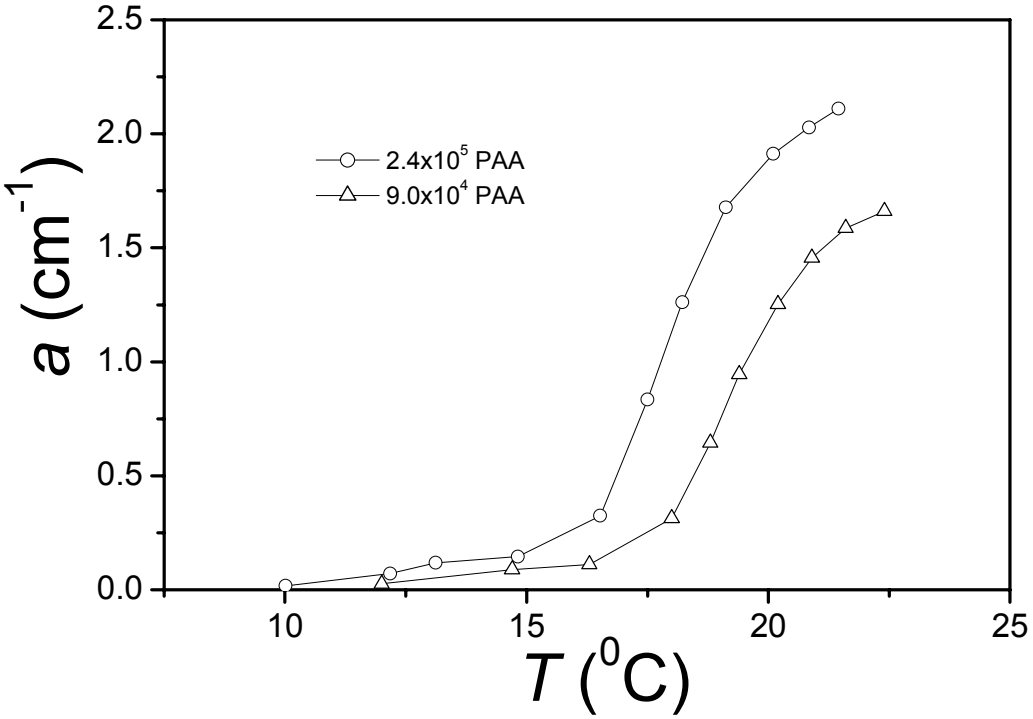

Figure 6.3. The turbidity of the HPC/PAA for two different PAA molecular weights at 0.3wt%HPC and 1.0wt%PAA.

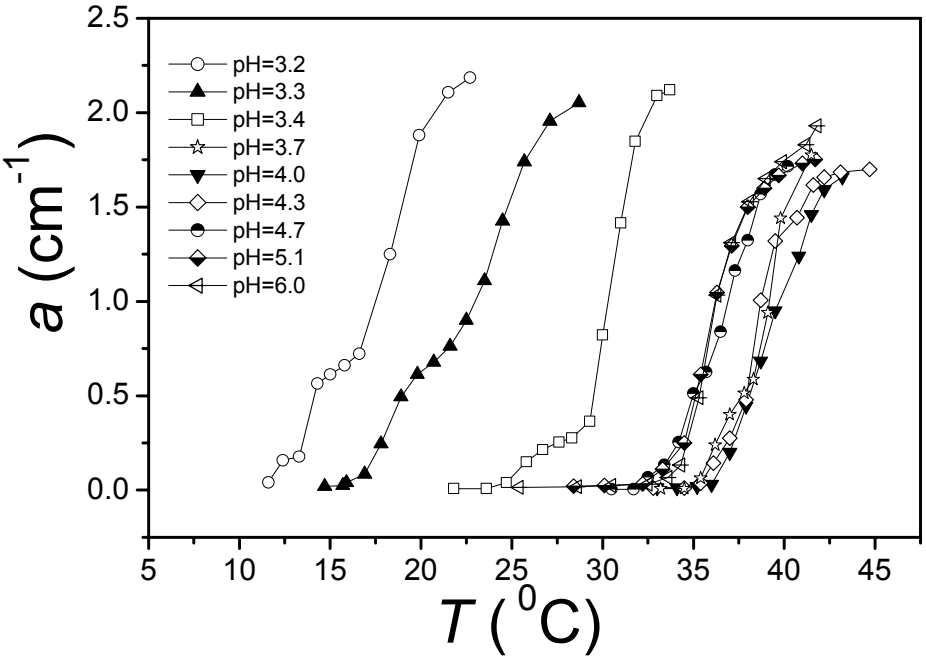

Figure 6.4a. The turbidity of the HPC/PAA for different pHs at 0.6wt% HPC and 1.0wt% PAA.

pH effect on the LCST of the HPC-PAA complex. Figure 6.4a shows the phase transition behavior of the complexes at various pH values and Figure 6.4b summarizes the LCST as a function of pH values. The data of the LCST vs pH in Figure 6.4b may be divided into two region: (I) below pH=4.0 and (II) above pH = 4.0. In the first region (pH<4.0), poly(acrylic acid) is a weak acid and is in the molecular state at pH< pK_a (=4.7). The LCST of the complex shifts to lower temperature upon the decrease of pH. This is caused by stronger hydrogen bonding as the pH value decreases. At pH=3.2, the LCST of the complex is 16 ^{0}C, in comparison with 41^{0}C for the pure HPC solution. In the second region (pH>4.0), it is found that the LCST decreases with the increase of the

pH value. When the pH = 4.0, the phase transition behavior of the HPC-PAA complex is close to that of 1 wt. % HPC solution without PAA. This is attributed to the disrupted hydrogen bonding between HPC and PAA. As the pH increases further, the LCST decreases again. This could be caused by the salt effect of the totally ionized poly(acrylic acid).

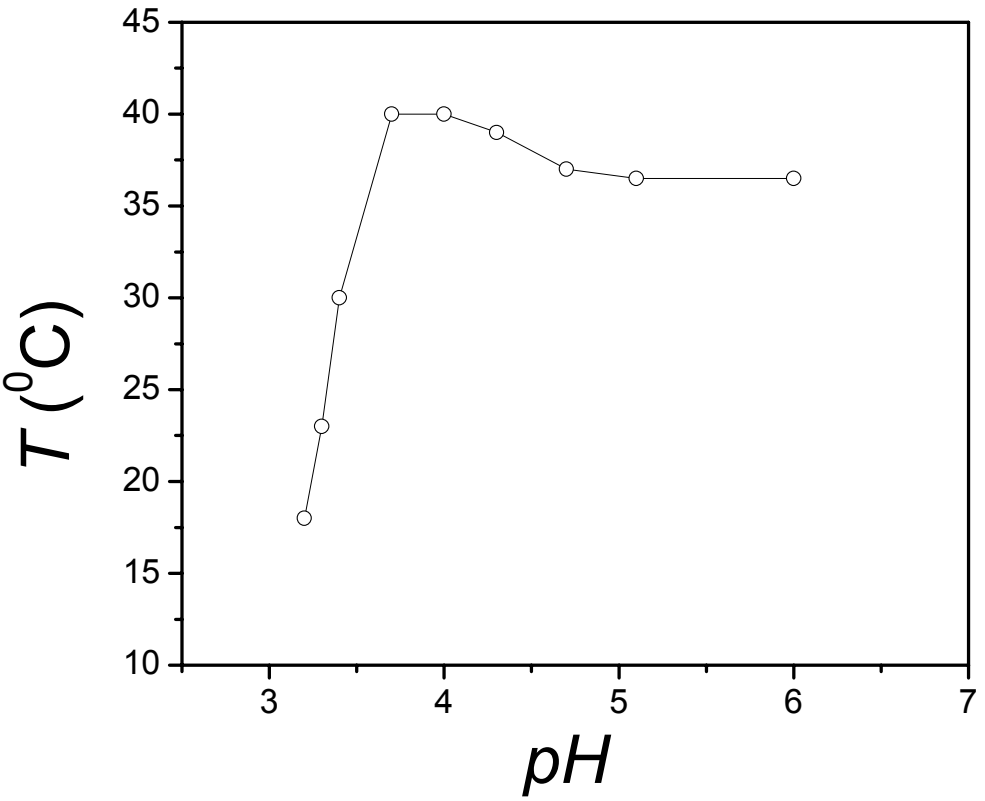

Figure 6.4b. The LCST of the HPC/PAA for different pHs at 0.6wt% HPC and 1.0%wt PAA.

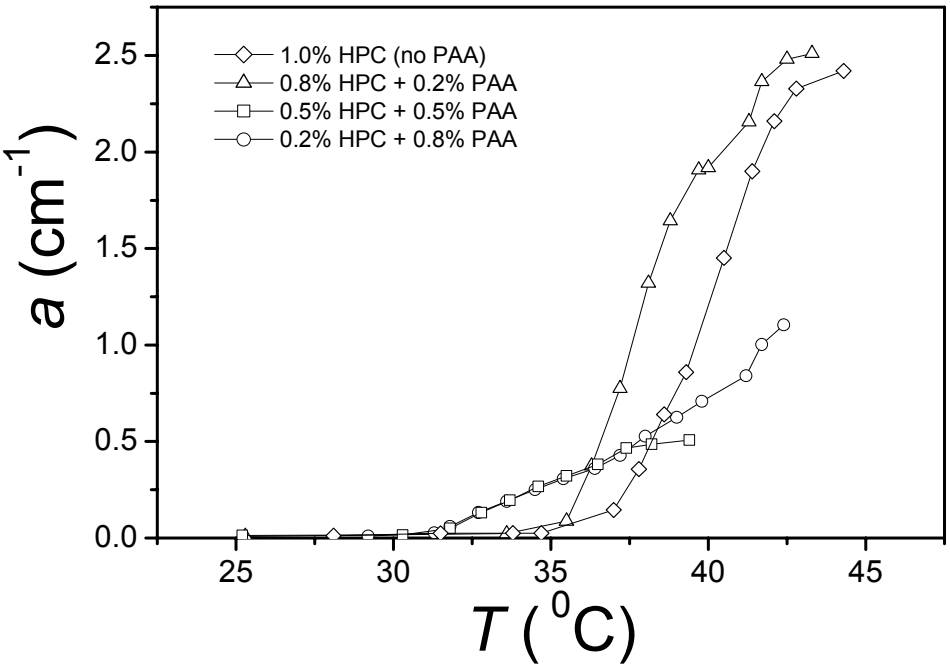

Figure 6.5. The turbidity of the 1.0wt% HPC/PAA at pH=7.4.

A previous study has shown that the LCST of the non-ionic HPC polymer can be shifted to a lower temperature by adding low molecular salt such as NaCl into the solution. [38] Iliopoulos[32] and co-worker have discussed the phase separation of the complex in which one polymer component is a polyelectrolyte such as poly(sodium acrylate) and the other is a non-ionic polymer such as the polyvinylpyrrolidone. To our knowledge, this is the first time that the salt effect of the ionized polyelectrolyte PAA on the LCST of the HPC-PAA complex has been revealed. To further demonstrate this effect, turbidity of a HPC-PAA complex with 1.0 wt% has been measured in PBS buffered solution at pH 7.4. The results is given in Figure 6.5. As the PAA concentration

increases, the LCST of the complex decreases. The magnitude of the change of the turbidity for higher PAA concentration (0.5 wt % and 0.8 wt %) is much smaller than that of 0.2% PAA concentration. Furthermore, it was found that the HPC/PAA at 0.5wt% and 0.8 wt% was unstable above the LCST and slowly precipitated. We attributed the shifting LCST of the HPC-PAA complex at pH=7.4 to the salt effect of the ionized polyelectrolyte PAA.

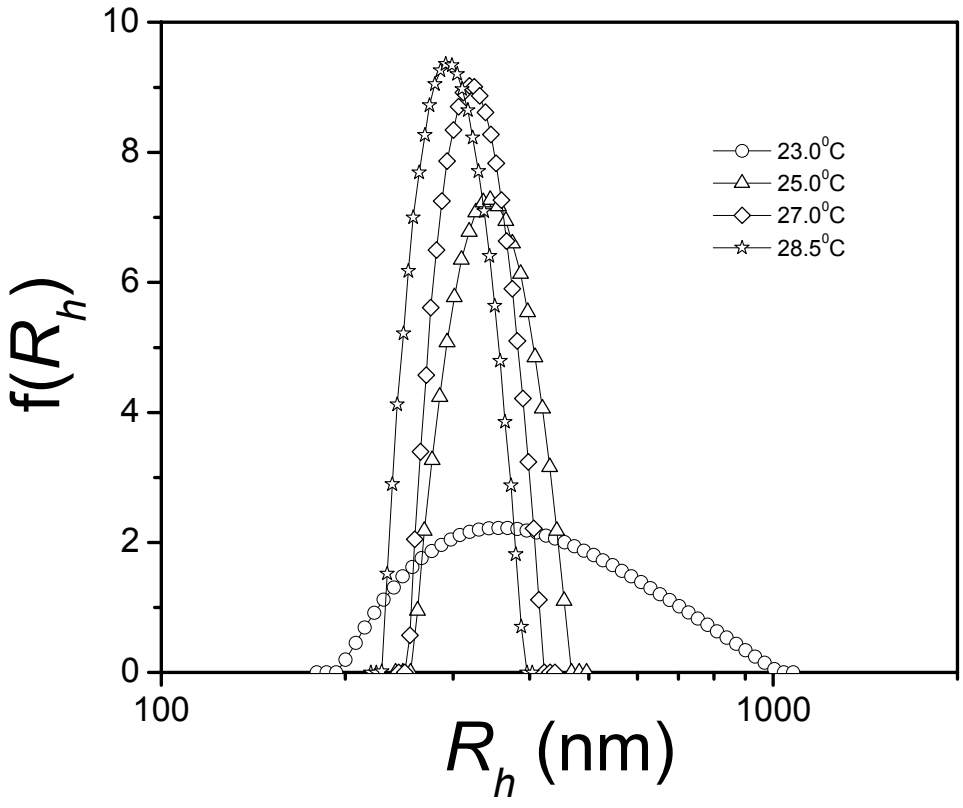

Figure 6. 6a. Hydrodynamic radius distributions ($f(R_h)$) of self-assembly HPC/PAA nanoparticles (C=1.6×10^{-5}g/ml) at pH=3.2.

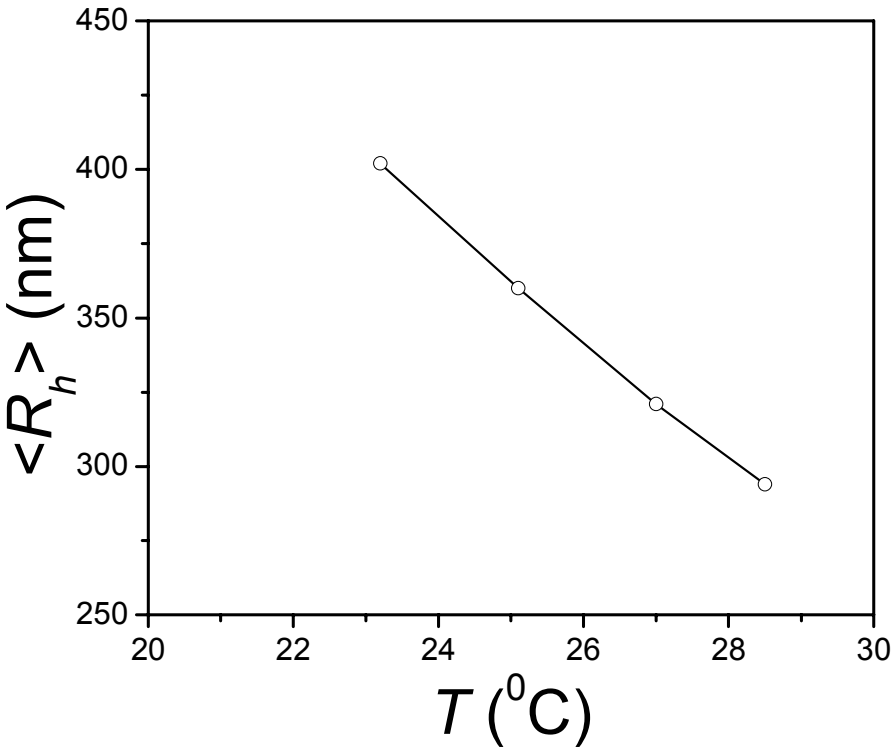

Figure 6.6b. Average hydrodynamic radius < R_h > of self-assembly HPC/PAA nanoparticles at pH=3.2.

Complexation in very dilute HPC/PAA Solution The phase transition behavior of the HPC/PAA complex discussed above was studied in a relatively high polymer concentration around 1 wt %. Here we report results of the HPC-PAA in very dilute polymer solution. As revealed by dynamic light scattering in Figure 6.6a, the HPC-PAA at polymer concentration of 1.6×10^{-5} g/ml can still form a complex at room temperature at pH=3.2. It is noted that the complex has a narrowly distributed hydrodynamic radius. This narrow distribution showes that the interpolymer hydrogen bonding of the dilute

HPC/PAA solutions at pH=3.2 can cause the decrease of the LCST, so they can aggregate into nanospheres at room temperature. In contrast, the HPC in dilute aqueous solution without PAA as a complexation agent would form nanospheres above 41 ^{0}C.[15] In addition, the hydrodynamic radius given in Figure 6.6b of the HPC-PAA complex in dilute polymer solution at pH=3.2 decreases as the environmental temperature increases within the range of temperatures studied.

Surfactant-free synthesis of PAA microgels based on interpolymer complexation. Previously, the PAA microgels and their derivatives were synthesized using inverse microemulsion polymerization [39, 40] with large amounts of organic solvent and surfactants. In practice, complete removal of the solvent and surfactants from the resultant polymeric particles is difficult, if not impossible. Here, a new method of preparing PAA microgels is proposed and demonstrated. The central idea is based on the HPC-PAA complexation in water through hydrogen bonding. At the beginning of polymerization, the PAA chains form a complex with the HPC chains at low pH. Then the PAA can aggregate around the complexes to form microgels.

To demonstrate this idea, we have prepared PAA microgels by mixing 2.0 g of 99wt% acrylic acid (AA), 10g of 1% HPC, and N, N'-methyleneacrylamide as a crosslinker in 68 g distilled and deionized water. The solution was stirred at 26 ^{0}C under nitrogen for 50 minutes. Then, 50 mg of ammonium persulfate and 50 mg of TEMED dissolved in 10 g of deionized water, respectively, were added into the solution to initialize polymerization. The reaction was carried out at 26 ^{0}C for 80 minutes.

The size and size distribution of the resultant PAA microgels at pH=3.2 and pH=7.4, characterized by dynamic light scattering measurement, are given in Figure 6.7. The average hydrodynamic radius $<R_h>$ at pH=3.2 is smaller than at pH=7.4. Decreasing particle size is caused by strong hydrogen bonding of the PAA at pH=3.2. As the microgels were at pH=3.2, the loose surface chains may collapse, resulting in a narrower particle size distribution. In two cases, the single particle size distribution peak showed that the HPC macromolecular chains were inside the PAA microgels.

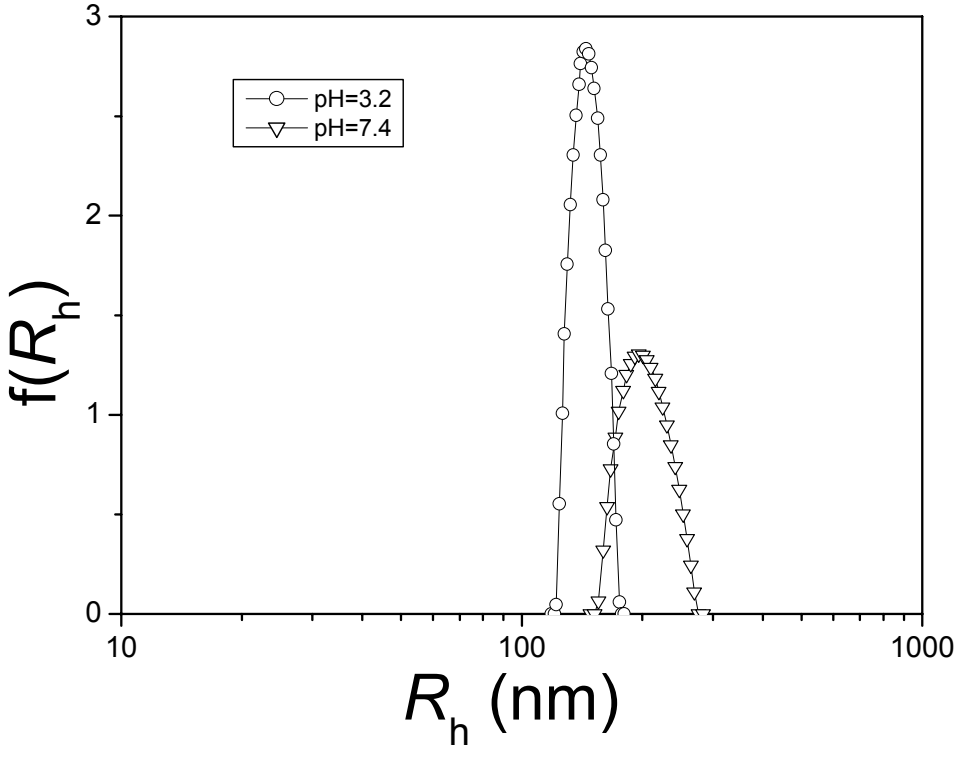

Figure 6.7. Hydrodynamic radius distribution ($f(R_h)$) of PAA microgel particles ($C=1.32\times10^{-5}$ g/mL) in pH=3.2 and pH=7.4 at 25^0C.

6.4 CONCLUSION

The phase transition behavior of the hydroxypropyl cellulose (HPC) and poly(acrylic acid) complex system in water has been investigated. The LCST of the complex shifted to much lower temperature than that of the HPC without the PAA as a complaxation agent at pH=3.2. The decrease of the phase transition temperature is attributed to the strong hydrogen bonding between the HPC and PAA. The LCST of the complexes decreased with the increase of the molecular weight of either HPC or PAA. As the pH value increases from 4.0 to 7.4, the LCST of the HPC-PAA complex decreases. This may be due to the salt effect of the polyelectrolyte on the non-ionic polymer. The dilute HPC/PAA aqueous solution at pH=3.2 can form interpolymer complexation near room temperature, and the associated nanoparticle sizes decreased with increasing temperature. The complexation between HPC and PAA leads to a new method for the formation of surfactant-free nanoparticles at room temperature. Formation of PAA gel nanoparticles in the presence of a small amount of HPC was monitored by LLS and proven by seeing the size difference of the collapsed and swollen gel nanoparticles at pH higher and lower than pK_{α}.

REFERENCES

(1) Bekturov, E. A.; Bimendina, L.A. *Adv. Polym. Sci*. **1981**, *41*, 99.

(2) Tshuchi, E; Abe, K. *Adv. Polym. Sci*. **1982**, *45*, 1.

(3) Wang, Y.; Morawetz, H. *Macromolecules* **1989,** *22,* 164.

(4) Jiang, M.; Li, M.; Xiang, M.; Zhou, H. *Adv. Polym. Sci.* **1998,** *146,* 121.

(5) Okano,T. *Adv. Polym. Sci*. **1993**, *110*, 179.

(6) Koussathana, M.; Lianos, P; Staikos, G. *Macromolocules* **1997,** *30*, 7798.

(7) Huang, X.D.; Goh, S. H. *Macromolecules* **2000**, *33*, 8894.

(8) Lele, B.S.; Hoffman, A. S. J. *J. Controlled Release* **2000**, *69*, 237.

(9) Dan,Y.; Chen, S. Y.; Zhang, Y. F.; Xiang, F. R. *J. Polym. Sci. Part B-Polym. Phys*. **2000,** *38*, 1069.

(10) Kaczmarek, H.; Szalla, A.; Kaminska, A. *Polyme*r **2001**, *42*, 6057.

(11) Iliopoulos, I.; Audebert, R. *Macromolecules* **1991**, *24*, 2566.

(12) Prevysh, V. A.; Wang, B. C.; Spontak R. S. *Coll. Polym. Sci.* **1996**, *274*, 532.

(13) Aoki, T.; Kawashima, M.; Katono, H.; Sanui, K.; Ogata, N.; Okano, T.; Sakurai, Y. *Macromolecules* **1994**, *27*, 947.

(14) Karayanni, K.; Staikos, G. *Eur. Polym. J.* **2000**, *36*, 2645.

(15) Gao, J.; Haidar, G.; Lu, X. H.; Hu, Z. B. *Macromolecules* **2001**, *34*, 2242.

(16) Harsh, D.C.; Gehrke, S.H. *J. Controlled Release* **1991**, *17,* 175.

(17) Lu, X. H.; Hu, Z. B.; Gao, J. *Macromolecules* **2000**, *33*, 8698.

(18) Pather; S. I.; Robinson, J. R.; Eichman, J.D.; Khankari, R. K.; Hontz, J.; Gupte, S.V. *US 6391335*, **2002**.

(19) Barkalow, D. G.; Richey, L. C.; Zuehlke, J. W. *US 6303159,* **2001**.

(20) Slepian, M. J.; Massia, S. P. *US 6290729,* **2001**.

(21) Zhou, S.; Chu, B. *J. Phys. Chem. B* **1998**, *102*, 1364.

(22) Xue, W.; Hamley, I. *Polymer* **2002**, *43*, 3069.

(23) Feil, H.; Bae, Y. H.; Jan, F.; Kim, S. W. *Macromolecules*, **1993**, *26*, 2496.

(24) Nikolaeva, O.; Budtova, T.; Alexeev, V.; Frenkel, S. *J. Polym. Sci.: Part B: Polymer Physics* **2000**, *38*, 1323.

(25) Nikolaeva, O. V.; Budtova, T. V.; Kalyuzhnaya, L. M.; Bel'nikevich, N. G.; Vlasova, E. N.; Frenkel, S. Y. *Polymer Science*, *Ser. A* **1999**, *41*, 771.

(26) Budtova, T. V.; Suleimenov, I. E.; Frenkel, S. Y. *J. Polym. Sci.: Part A: Polymer Chemistry* **1994**, *32*, 281.

(27) Doseva, V; Senkov, S.; Baranovsky, Y. V. *Polymer* **1997,** *38*, 1339.

(28) Joshi, A.; Ding, S.; Himmelstein, K. J. *US 5252318*, **1993**.

(29) Staikos, G.; Bokias, G.; *Macromol. Chem.* **1991**, *192*, 2649.

(30) Subotic, D. V.; Ferouson, J.; Warren, B. C. H. *Eur. Polym. J.* **1991**, *27*, 61.

(31) Budtova, T.; Navard, P. *Macromolecules* **1996**, *29*, 3931.

(32) Hu, Z. B.; Lu, X. H.; Gao, J.; Wang, C. *Advanced Materials* **2000,** *12***,** 1173.

(33) Li, Y.; Wang,G.; Hu, Z. *Macromolecules* **1995**, *28*, 4194.

(34) Yu, X.; Tanaka, A.; Tanaka, K.; Tanaka, T. *J. Chem. Phys*. **1992**, *97*, 780.

(35) Karlstrom, G.; Carlsson, A.; Lindman, B. *J. Phys. Chem.* **1990**, *94*, 5005.

(36) Chen, H.; Morawetz, H. *Macromolecules* **1985**, *18*, 1829.

(37) Chen, H.; Morawetz, H. *Eur. Polymer* **1983,** *19,* 923.

(38) Drummond, C. J.; Albers, S.; Furlong, D. N. *Coll. Surf.* **1992**, *62*, 75.

(39) Kriwet, B.; Walter, E.; Kissel, T. *J. Controlled Release* **1998**, *56*, 149.

(40) Bouillot, P.; Vincent, B. *Colloid Polym. Sci*. **2000**, *278*, 74.

CHAPTER 7
CONCLUSION

This dissertation investigates the synthesis and properties of novel polymer hydrogel nanoparticles and nanostructured hydrogels. The hydrogel nanoparticles include FDA-approved HPC microgels,[1, 2] hydrophilic PVA nanoparticles, [3] monodisperse NIPA-co-HEAC nanoparticles, [4] surfactant-free hydrophilic PAA microgels. [5] Based on these nanoparticles, several nanostructed hydrogels[3, 4, 6, 7] were designed. The main conclusions of this dissertation are described as follows:

(1) HPC microgels have been synthesized for the first time by chemically crosslinking hydroxypropyl cellulose (HPC) linear macromolecules. [1] The controllable synthesis parameters – surfactant concentration, HPC concentration and reaction temperature – were varied to determine the effects on the size and size distribution of the microgels as monitored using laser light scattering techniques. It was found that the microgels can form only above the CMC of the DTAB surfactant at the LCST. As the HPC concentration increases from 0.1 wt% to 0.3 wt%, size distribution becomes significantly broader. Furthermore, the reaction temperature plays an important role for the size distribution: upon the increase of the temperature above the LCST, the particle size increases quickly. The formation of microgels may be explained by the balance between hydrophobic interactions between HPC polymer chains and inter-micelle electrostatic repulsion. The swelling and phase transition properties of the resultant

HPC microgels are analyzed using both static and dynamic light scattering techniques as a function of temperature at various crosslinker concentrations. It is found that the increase in the crosslinker density reduces the shrinkage extent and increases the transition temperature. The dilute HPC microgel particles with concentration of 8.94×10^{-6} g/ml form a stable colloidal dispersion at room temperature and at 44°C ($>T_c$), probably due to steric effects. In the aqueous solution of physiological salt concentration, the phase transition of the HPC microgels occurs at about 39°C, which corresponds to fever temperature of the human body. Combining the temperature-responsive volume change, bio-compatibility of the HPC, and uniform and small size, the HPC microgels could be particularly useful in controlled drug delivery applications.

(2) A new class of nanostructured polymer gel has been synthesized by crosslinking gel nanoparticles through covalent bonds between functional groups on the surfaces of neighboring particles in solutions. [3, 6] Thus, these gels have two levels of structural hierarchy: the primary network is closslinked polymer chains in each nanoparticle, while the secondary network is crosslinked nanoparticles as a whole. With such a unique structure, they have new properties that conventional gels do not have, including high surface area, controlled heterogeneity in the nanoscale, and uniform and easily tunable mesh sizes. Architectures of nanostructured gels could be easily tailored by selecting different gel nanoparticles and crosslinking agents. Several applications of gel nanoparticle networks are presented in this paper, including a nanoparticle network with a fast shrinking rate, a light scattering-colored nanoparticle network, and a co-nanoparticle network as a potential multi-functional drug delivery carrier.

(3) Hydrogel opals have been synthesized by covalently bonding self-assembled hydrogel nanoparticles. [4, 7] The covalent bonding contributes to the mechanical and thermal stability of the assemblies, while self-assembly provides the bulk hydrogels with crystal structures which diffract light, resulting in colors. Several applications of crystal hydrogels are presented in this thesis, including a gel sensor whose color can be tuned by either temperature or an electric field, a gel "opal" that displays a striking iridescence and is wet and elastic, and a gel display whose iridescent pattern can be made either visible or invisible by simply switching temperature. This work may lead to technological applications, ranging from sensors and displays to home decoration.

(4) The phase transition behavior of the hydroxypropyl cellulose (HPC) and poly(acrylic acid) complex system in water has been investigated. [5] The LCST of the complex shifted to much lower temperature than that of the HPC without the PAA as a complaxation agent at pH=3.2. The decrease of the phase transition temperature is attributed to the strong hydrogen bonding between the HPC and PAA. The LCST of the complexes decreased with the increase of the molecular weight of either HPC or PAA. As the pH value increases from 4.0 to 7.4, the LCST of the HPC-PAA complex decreases. This may be due to the salt effect of the polyelectrolyte on the non-ionic polymer. The dilute HPC/PAA aqueous solution at pH=3.2 can form interpolymer complexation around room temperature, and the associated nanoparticle sizes decreased with increasing temperature. The complexation between HPC and PAA leads to a new method for the formation of surfactant-free nanospheres at room temperature. Formation of PAA gel microspheres in the presence of a small amount of HPC was

monitored by LLS and proven by seeing the size difference of the collapsed and swollen gel microspheres at pH higher and lower than pK_{α} .

REFERENCES

(1) Lu, X. H.; Hu, Z. B.; Gao, J. *Macromolecules* **2000**, *33*, 8698.

(2) Gao, J.; Haidar, G.; Lu, X. H.; Hu, Z. B. *Macromolecules* **2001**, *34*, 2242.

(3) Hu, Z.; Lu, X.; Gao, J. Wang, C. *Advanced Materials* **2000**, *12*, 1173.

(4) Hu, Z.; Lu, X.; Gao, J. *Advanced Materials* **2001**, *13*, 1783.

(5) Lu, X.; Hu, Z.; Schwartz, J. submitted to *Macromolecules*.

(6) Hu, Z.; Lu, X.; Gao, J. " Synthesis and uses of polymer gel nanoparticle network", *U. S. Patent, Disclosure filed* **(August 2001).**

(7) Hu, Z.; Lu, X.; Gao, J. " Synthesis and composition of crystal hydrogels" *U. S. Patent*, *Disclosure filed* **(November 2001**).

BIBLIOGRAPHY

(1) Ahlnas, T.; Karlstrom, G.; Lindman, B. *J. Phys. Chem.* **1987**, *91*, 4030.

(2) Allcock, H. R.; Lampe, F. W. *Contemporary Polymer Chemistry*, 2nd edition; Prentice-Hall, Ins.: New Jersey, **1990**.

(3) Anbergen, U.; Oppermann, W. *Polymer* **1990**, *31*, 1854.

(4) Antionietti, M.; Pakula, T.; Bremser, W. *Macromolecules* **1995**, *28*, 4227.

(5) Aoki, T.; Kawashima, M.; Katono, H.; Sanui, K.; Ogata, N.; Okano, T.; Sakurai Y. *Macromolecules* **1994**, *27*, 947.

(6) Barkalow, D. G.; Richey, L. C.; Zuehlke, J. W. *US 6303159*, **2001**.

(7) Beebe, D. J.; Moore, J. S.; Bauer, J. M.; Yu, Q.; Liu, R. H.; Devadoss, C.; Jo, B. H. *Nature* **2000,** *404***,** 588.

(8) Bekturov, E. A.; Bimendina, L.A. *Adv. Polym. Sci*. **1981**, *41*, 99.

(9) Berne, B. J.; Pecora, R. *Dynamic Light Scattering*; John Wiley & Sons, Inc: New York **1976**.

(10) Bouillot, P.: Vincent, B. *Colloid Polym. Sci*. **2000**, *278*, 74

(11) Bradna, P.; Quadrat, Q.; Snuparck, *J. Colloid Polym. Sci.* **1995**, *273*, 324.

(12) Brown, W. *Dynamic Light Scattering*; Oxford University Press: Oxford, **1993**.

(13) Budtova, T.; Navard, P. *Macromolecules* **1996**, *29*, 3931.

(14) Budtova, T. V.; Suleimenov, I. E.; Frenkel, S. Y. *J. Polym. Sci.: Part A: Polymer Chemistry* **1994**, *32*, 281.

(15) Chen, G.; Hoffman, A. S. *Nature* **1995,** *373,* 49.

(16) Chen, H.; Morawetz, H. *Macromolecules* **1985**, *18*, 1829.

(17) Chen, H.; Morawetz, H. *Eur. Polymer* **1983,** *19,* 923.

(18) Chu, B. *Laser Light Scattering*, 2nd ed.; Academic Press: New York, **1991**.

(19) Clark, N. A.; Hurd, J.; Ackerson, B. J. *Nature* **1979**, *281*, 57.

(20) Dan,Y.; Chen, S. Y.; Zhang, Y. F.; Xiang, F. R. *J. Polym. Sci. Part B-Polym. Phys*. **2000,** *38*, 1069

(21) Doseva, V; Senkov, S.; Baranovsky, Y. V. *Polymer* **1997,** *38*, 1339.

(22) Drummond, C. J.; Albers, S.; Furlong, D. N. *Colloids Surf.* **1992**, *62*, 75.

(23) Feil, H.; Bae, Y. H.; Jan, F.; Kim, S. W. *Macromolecules*, **1993**, *26*, 2496.

(24) Frank, M.; Burchard, W. *Makromol. Chem. Rapid Commun.* **1991**, *12*, 64.

(25) Gao, J.; Haidar, G.; Lu, X. H.; Hu, Z. B. *Macromolecules* **2001**, *34*, 2242.

(26) Gong, J. P.; Okuzaki, H.; Osada, Y.; *Macromol. Chem. Phys*. **1994**, *195*, 1871.

(27) Harsh, D.C.; Gehrke, S. H. *J. Controlled Release* **1991**, *17*, 175.

(28) Hellweg, T.; Dewhurst, C. D.; Bruckner, E.; Kratz, K.; Eimer, W. *Colloid Polym* Sci. **2000**, 278, 972.

(29) Hirotsu, S. *Japn. J. Appl. Phys*. **1985**, *24*, 396.

(30) Hirotsu, S.; Hirokawa, Y.; Tanaka, T. *J. Chem. Phys*. **1987**, *87*, 1392.

(31) Holtz, J. H.; Asher, S. A. *Nature* **1997,** *389*, 829.

(32) Hormnirun, P.; Sirivat, A.; Jamieson, A. M. *Polymer* **2000**, *41*, 2127.

(33) Hu, Z.; Chen, Y.; Wang, C.; Zheng, Y.; Li, Y. *Nature* **1998**, *393*, 149.

(34) Hu, Z.; Lu, X.; Gao, J.; Wang, C. *Advanced Materials* **2000**, *12*, 1173.

(35) Hu, Z.; Lu, X.; Gao, J. *Advanced Materials* **2001**, *13*, 1783.

(36) Hu, Z.; Lu, X.; Gao, J. " Synthesis and uses of polymer gel nanoparticle network", *U. S. Patent, Disclosure filed* **(August 2001)**

(37) Hu, Z.; Lu, X.; Gao, J. " Synthesis and composition of crystal hydrogels" U. S. Patent, Disclosure filed **(November 2001**)

(38) Hu, Z.; Zhang, X.; Li, Y. *Science* **1995,** *269*, 525.

(39) Iliopoulos, I.; Audebert, R. *Macromolecules* **1991**, *24*, 2566.

(40) Inomata, H.; Goto, S.; Otake, K.; Saito, S. *Langmuir* **1992**, *8*, 687.

(41) Jethmalani, J. M.; Ford, W. T.; Beaucage, G. Langmuir, **1997**, *13*, 3338.

(42) Jethmalani, J. M.; Sunkara, H. B.; Ford, W. T.; Willoughby, S. L.; Ackerson, B. J. *Langmuir* **1997**, *13*, 2633.

(43) Jiang, M.; Li, M.; Xiang, M.; Zhou, H. *Adv. Polym. Sci.* **1998,** *146,* 121.

(44) Joshi, A.; Ding, S.; Himmelstein, K. J. *US5252318,* **1993**.

(45) Kabra, B. G.; Gehrke, S. H.; Spontak, R. J. *Macromolecules* **1998**, *31*, 2166.

(46) Kaczmarek, H.; Szalla, A.; Kaminska, A. *Polyme*r **2001**, *42*, 6057.

(47) Kamenetzky, E. A.; Magliocco, L. G.; Panzer, H. P. *Science* **1994,** *263***,** 207.

(48) Karlstrom, G. *J. Phys. Chem.* **1985**, *89*, 4962.

(49) Karlstrom, G.; Carlsson, A.; Lindman, B. *J. Phys.Chem.* **1990**, *94*, 5005.

(50) Kiser, P. F.; Wilson, G.; Needham, D.; *Nature* **1998,** *394*, 459.

(51) Koussathana, M.; Lianos, P; Staikos, G. *Macromolocules* **1997,** *30*, 7798.

(52) Krieger, I. M.; O'Neill, F. M. *J. Amer. Chem. Soc.* **1968**, *90*, 3115.

(53) Kriwet, B.; Walter, E.; Kissel, T. *J. Controlled Release* **1998**, *56*, 149.

(54) Lashkevich, O. V.; Dyagileva, A. B.; Chernoberezhskii, Y. M. *Colloid J.* **1997**, *59*, 467.

(55) Lele, B.S.; Hoffman, A. S. J. *J. Controlled Release* **2000**, *69*, 237.

(56) Li, Y.; Tanaka, T. *J. Chem. Phys.* **1990**, *40*, 820; *J. Chem. Phys*. **1990,** *92,* 1365.

(57) Li, Y.; Wang, G.; Hu, Z. *Macromolecules* **1995,** *28*, 4194.

(58) Lu, X.; Hu, Z.; Gao, J. *Macromolecules* **2000**, *33*, 8698.

(59) Lu, X.; Hu, Z.; Schwartz, J. submitted to *Macromolecules*

(60) Murry, M. J.; Snowden, M. J. *Adv. Colloid Interf. Sci.* **1995**, *54*, 73.

(61) Neyret, S.; Vincent, B. *Polymer* **1997**, *38*, 6129.

(62) Nikolaeva, O.; Budtova, T.; Alexeev, V.; Frenkel, S. *J. Polym. Sci.: Part B: Polymer Physics* **2000**, *38*, 1323.

(63) Okano,T. *Adv. Polym. Sci*. **1993**, *110*, 179.

(64) Osada, Y.; Gong, J. P. *Adv. Mater*. **1998**, *10,* 827.

(65) Oya, T.; Enoki, T.; Grosberg, A. Y.; Masamune, S.; Sakiyama, T.; Takeoka, Y.; Tanaka, K.; Wang, G.; Lilmaz, Y.; Feld, M. S.; Dasari, R.;Tanaka, T. *Science* **1999**, *286*, 1543.

(66) Pather; S. I.; Robinson, J. R.; Eichman, J.D.; Khankari, R. K.; Hontz, J.; Gupte, S.V. *US 6391335*, **2002**.

(67) Pelton, R. *Adv. Colloid Interf. Sci.* **2000**, *85*, 1.

(68) Pelton, R.H.; Chibanate, P. *Colloids Surf.* **1986**, *120*, 247.

(69) Peppas, N. A. *Hydrogels in Medicine and Pharmacy,* CRC Press: FL, **1987**.

(70) Peppas, N. A.; Langer, R. *Science* **1994,** *263*, 1715.

(71) Prevysh, V. A.; Wang, B. C.; Spontak R. S. *Coll. Polym. Sci.* **1996**, *274*, 532.

(72) Pusey, P. N.; van Megen, B. *Nature* **1986**, *320*, 340.

(73) Sahoo, S. K.; De, T. K.; Ghosh, P. K.; Maitra, A. *J. Coll. Interf. Sci.* **1998**, *206*, 361.

(74) Sanders, J. V. *Nature* **1964**, *204*, 1151.

(75) Sasa, N.; Yamaoks, T. *Adv. Mater.* **1994**, *6*, 417.

(76) Saunders, B. R.; Vincent, B. *Adv. Colloid Interf. Sci.* **1999**, *80*, 1.

(77) Schild, H. G. *Prog. Polym. Sci*. **1992**, *17*, 163.

(78) Senff, H.; Richtering, W. *J. Chem. Phys*. **1999**, *111*, 1705.

(79) Siegel, R. A.; Firestone, B. A. *Macromolecules* **1988**, *21*, 3254.

(80) Slepian, M. J.; Massia, S. P. *US 6290729,* **2001**.

(81) Staikos, G.; Bokias, G.; *Macromol. Chem.* **1991**, *192*, 2649.

(82) Subotic, D. V.; Ferouson, J.; Warren, B. C. H. *Eur. Polym. J.* **1991**, *27*, 61.

(83) Tanaka, T. *Phys. Rev. Lett*. **1978**, *40*, 820.

(84) Tanaka, T. *Experimental Methods in Polymer Science*; Academic Press, **2000**.

(85) Tanaka, T.; Nishio, I.; Sun, S. T.; Ueno-Nishio, S. *Science* **1982**, *218*, 467.

(86) Tshuchi, E; Abe, K. *Adv. Polym. Sci*. **1982**, *45*, 1

(87) Wang, Y.; Morawetz, H. *Macromolecules* **1989,** *22,* 164.

(88) Weissman, J. M.; Sunkara, H. B.; Tse, A. S.; S. A. Asher, *Science* **1996**, *274*, 959.

(89) Winnik, F.M.; Tamai, N.; Yonezawa, J.; Nishimura, Y.; Yamazaki, I. *J. Phys. Chem.* **1992**, *96*, 1967.

(90) Wu, C. *Polymer* **1998**, *39*, 4609.

(91) Wu, C.; Chan, K. K.; Xia, K. Q. *Macromolecules* **1995**, *28*, 1032.

(92) Xia, Y.; Gates, B.; Yin, Y.; Lu, Y. *Adv. Mater*. **2000**, *12*, 693.

(93) Xia, Y. *Adv. Mater*. **2001**, *13*, 369.

(94) Xue, W.; Hamley, I. *Polymer* **2002**, *43*, 3069.

(95) Yoshida, R.; Takahashi, T.; Ichijo, H. *Adv. Mater*. **1997**, *9*, 175.

(96) Yoshida, R.; Uchida, K.; Kaneko, Y.; Sakal, K.; Kikuchi, A.; Sakurai, Y.; Okano, T. *Nature* **1995,** *374*, 240.

(97) Zhang, G.; Wu, C. *J. Am. Chem. Soc.* **2001**, *123*, 1376.

(98) Zhou, S; Chu, B. *J. Phys. Chem*. **1998**, *102*, 1364.